DOI: 10.26599/FSHW.2026.9251078

Contents lists available at SciOpen

Food Science and Human Wellness

journal homepage: https://www.sciopen.com/journal/2097-0765

China Food Publishing Co.

Structural characteristics of a pectin from Gannan navel orange (*Citrus sinensis* Osbeck cv. Newhall) peels and its gastroprotective activity on alcohol-induced gastric mucosal lesions in rats

Yan-Bin Hao [a], Yuan Chen [a], Bin Zhang [a], Jia-Min Chen [a], Rui-Yun Chen [a], Jia-Lin Zhou [b], Jiang-Hong Luo [a], Qi Zou [a], Yi Yan [c], Xiao-Yin Wang [a, *]

[a] *School of Public Health and Health Management, Gannan Medical University, Ganzhou 341000, China*

[b] *The Third Affiliated Hospital of Gannan Medical University, Gannan Medical University, Ganzhou 341000, China*

[c] *First Affiliated Hospital of Gannan Medical University, Gannan Medical University, Ganzhou 341000, China*

ABSTRACT: In our previous study, a pectin NOP from Gannan navel orange (*Citrus sinensis* Osbeck cv. Newhall) peels has been gained. This study sequentially determines its structure using methylation analysis and NMR spectroscopy, and evaluates its gastroprotective activity against alcohol-induced gastric mucosal lesions (AGML) in rats. Meanwhile, the mechanism was explored by RNA-seq, western blot, 16S rRNA and untargeted metabolomics analyses along with correlation analyses and molecular docking. Results showed that NOP consisted of HG domain, RG-I domain and β-1,6-D-glucan structure. The side chains of RG-I domain were composed of →5)-α-L-Ara*f*-(1→, β-D-Gal*p*-(1→, →4)-β-D-Gal*p*-(1→ and →3,6)-β-D-Gal*p*-(1→ residues. NOP ameliorated gastric lesion, decreased inflammatory responses and protein expressions of inflammatory signaling pathways-related hub targets (Ccl2, Cxcl1, Icam1, Il6, Jun and Lif), changed gene expressions and metabolism of gastric tissues, and regulated gut microbiota in AGML rats. Moreover, gut microbiota biomarkers, biochemical indexes and differential metabolites affected by NOP showed significantly positive and negative correlations. Furthermore, the representative metabolites like hypoxanthine and the inflammatory signaling pathways-related hub targets exhibited good binding activities. It can be concluded that NOP is a candidate for alleviating AGML, exerting gastroprotection through inflammatory signaling pathways, gut microbiota and metabolites in AGML rats. This study provides theoretical basis for the exploitation and utilization of NOP in preventing AGML, and the future mechanism investigation.

Keywords: Gannan navel orange; Pectin; Structure; Gastroprotection; Multi-omics

1. Introduction

There are approximately 2.3 billion alcohol drinking populations worldwide, of which more than 3 million populations died from harmful use of alcohol, accounting for 5.3 percent of all deaths. Thereinto, digestive diseases accounted for 21.3% of alcohol-related deaths[1]. Alcohol is one of main aggressive factors to gastric mucosa, as large alcohol consumption in a short period of time can lead to alcohol-induced gastric mucosal lesions (AGML). The AGML usually appears as edema of different degrees, hyperemia, erosion,

***Corresponding author**
(X-Y Wang) xywang@gmu.edu.cn

Received 6 June 2025
Received in revised from 16 July 2025
Accepted 27 December 2025

bleeding, perforation, ulcer, tissue necrosis, etc. Once the gastric mucosa is damaged, the people's quality of life will be seriously affected. With no appropriate intervention, gastric mucosal lesions may develop into gastric cancer resulting in high mortality. Epidemiologic studies showed that more than 5% of new cancer diagnoses were related to alcohol consumption, and alcohol consumption is a high-risk factor for gastric cancer[2]. Therefore, the intervention of AGML is of great significance for improving people's quality of life and reducing social disease burden.

At present, gastric mucosal protective or anti-acids drugs are frequently used to intervene AGML. However, the usage doses are relatively large and their long-term uses often bring many side effects, such as osteoporotic fracture, vitamin B_{12} deficiency and infection of digestive tract[3]. In view of this, it is necessary to find safer and more effective drug substitutes for the intervention of AGML. Polysaccharides, a kind of macromolecular substance widely existing in nature, possess various biological activities and are extensively utilized in food, healthcare product, and cosmetic industries. A large number of polysaccharides have been shown to alleviate AGML, and several of them exhibited stronger efficacies than gastric mucosal protective drugs[4], showing good potentials in alleviating AGML. The alleviations of polysaccharides against AGML might be related to many ways including anti-inflammatory. Previous studies have demonstrated that Nrf2, MAPK/NF-κB, MAPK-p38, JAK/STAT and IκB/NF-κB signaling pathways involved in the anti-inflammatory effects of polysaccharides during they alleviated AGML[5-9]. However, it is well-known that most polysaccharides cannot be hydrolyzed into oligosaccharides or monosaccharides under the actions of gastrointestinal digestive enzymes and digestive fluids. While, there are approximately 10^{13}~10^{14} gut microbiota in the intestinal tract. The complex polysaccharides that cannot be digested or digested completely are converted to short-chain fatty acids and other metabolites by the gut microbiota, as gut microbiota can encode a large number of carbohydrate active enzymes that degrade complex polysaccharides[10]. Then, the produced short-chain fatty acids and other metabolites play important roles in promoting human health. In this light, it remains uncertain whether polysaccharides alleviate AGML by modulating the above signaling pathways through the metabolites to exert anti-inflammatory effects.

Recently, polysaccharides from *Sarcodon aspratus* or small black soybean have been shown to regulate gut microbiota, alter serum metabolites and reduce inflammatory responses, during improving acetic acid- or water immersion-induced gastric mucosal lesions in rats[11,12]. Meanwhile, the alterations of small black soybean polysaccharide on serum metabolites were correlated with the regulations on gut microbiota[11]. In terms of AGML, the changes of a refined *Evodiae fructus* polysaccharide on serum and liver metabolites were obviously related to its activation on Keap1/Nrf2/HO-1 signaling pathway and reduction on inflammatory responses, during ameliorating AGML in mice[13]. A pectic polysaccharide from wax gourd peel might improve AGML in mice through regulating metabolic pathway[14]. Moreover, a low-molecular-weight β-glucan of *Hericium erinaceus* could modulate gut microbiota when exhibiting gastroprotective effects in AGML mice[15]. The protective effects of polysaccharides from *Dendrobium officinale* on AGML had potential links with the regulations on gut microbiota[9]. A purified fraction from refined *Evodiae fructus*

showed significant correlations among its regulations on gut microbiota and serum metabolites, activation on PPARγ and reduction on inflammatory responses, during mitigating AGML in rats[16]. Furthermore, the findings of Li *et al*[17] have implied that polysaccharides from *Hippophae rhamnoides* L. might protect the integrity of gastric mucosa and tight junctions by modulating microbiota-derived metabolites in AGML rats. Based on the above evidence, we propose the following hypothesis: polysaccharides can regulate the gut microbiota to produce beneficial metabolites, which in turn modulate inflammatory pathways to exert anti-inflammatory effects, thereby alleviating AGML.

Gannan navel orange (*Citrus sinensis* Osbeck cv. Newhall), a national geographical indication product in China, is extensively grown in Ganzhou City, Jiangxi Province, due to intense fragrance, nutrient-rich and delicious taste[18]. A large amount of Gannan navel orange peel is generated during juice processing as well as daily consumption[19]. However, the left peels are often used as feed or directly discarded, which causes resources waste and environmental pollution. As we all known, apple and citrus peels are two typical sources for commercial pectins. Like other citrus fruits, the Gannan navel orange peels can also be used to produce pectins, which make up 20%-30% of the peels[20]. Currently, extraction of pectins from Gannan navel orange peels has attracted increasing attention[21,22]. However, studies on the structure and biological activity of the pectins are limited. In the past decade, many pectins have been demonstrated to possess gastroprotective activities against AGML in rats[23-26]. Although pectins from Gannan navel orange peels have been proven to exhibit hypoglycemic activity in our previous study[27], it is unclear whether they also have gastroprotective activity against AGML.

Hence, this study intends to characterize the structural features of a previously gained pectin from Gannan navel orange peels, and investigate its gastroprotective activity and the relevant mechanism against AGML in rats. Moreover, this study was designed to verify whether the aforementioned hypothesis is accurate or not. The findings offer a novel perspective for the gastroprotective mechanism research of polysaccharides such as pectins, and support the high-value utilization of Gannan navel orange peels.

2. Materials and methods

2.1 Materials and chemicals

The pectin (labelled as NOP) extracted from Gannan navel orange peels (picked from a local orchard (25.78°N, 114.81°E) in Ganzhou City, Jiangxi province, China) has been performed using acid water solution extraction, deproteinization and dialysis in our previous study[27]. NOP contained 68.1% uronic acid, had a molecular weight of 285.6 kDa, and showed an esterification degree of 72.0%. NOP was composed of rhamnose (Rha), arabinose (Ara), galactose (Gal), glucose (Glc), xylose (Xyl), mannose (Man) and galacturonic acid (GalA) in a mass percentage ratio of 2.1: 13.8: 17.8: 17.7: 2.3: 3.4: 42.9[27].

Sodium borohydride ($NaBH_4$), sodium borodeuteride ($NaBD_4$), N-cyclohexyl-N-[2-(4-methyl-1-oxa-4-azoniacyclohex-4-yl)ethyl]methanediimine,4-methylbenzenesulfonic acid, dichloromethane, trifluoroacetic acid, acetic anhydride, deuterium oxide (D_2O),

tris(trimethylsilyl)phosphate (TMSP), methanol and acetonitrile were bought from Aladdin Industrial Corp. (Shanghai, China). Rat ELISA kits of tumor necrosis factor-alpha (TNF-α) and interleukin 6 (Il6), anti-β-actin primary antibody and anti-rabbit-IgG-HRP secondary antibody were purchased from BOSTER (Wuhan, China). Primary antibodies of anti-Ccl2, anti-Cxcl1, anti-Icam1, anti-Il6, anti-Jun and anti-Lif were provided by Jiangsu Kinke Biological Research Center Co., Ltd. (Jiangsu, China). TRIzol, hematoxylin-eosin (HE) staining dye, BCA protein assay kit, 5×SDS-PAGE protein loading buffer and BeyoLytic™ mammalian active protein extraction reagents were gained from Beyotime Institute of Biotechnology (Shanghai, China). OMEGA Soil DNA Kit, NEBNext® Ultra^{TM} RNA Library Prep Kit, and TruSeq Nano DNA LT Library Prep Kit were respectively obtained from Omega Bio-Tek (Norcross, GA, USA), New England Biolabs (Ipswich, MA, USA) and Illumina (San Diego, CA, USA). All other used chemicals in this study were of analytical grade.

2.2 Animals

Eighteen male Sprague-Dawley (SD) rats (140-160 g, six weeks old) were provided by Hunan Slac Jingda Laboratory Animal Co. Ltd. (Certificate SCXK (xiang) 2019-0004, Hunan, China). The rats were housed in cages in a temperature (23 ± 2 °C) and humidity (50-65%) controlled room with 12 h light/12 h dark cycles. They had unlimited access to food and water. All of the experimental procedures followed the National Research Council's Guide for the Care and Use of Laboratory Animals, and were approved by the Experimental Animal Ethics Committee of Gannan Medical University (Certificate SYXK (gan) 2023-0004; Reference number: 2025308).

2.3 Structural characterization of NOP

2.3.1 Uronic acid reduction and methylation analysis

Uronic acid reduction and methylation analysis of NOP were sequentially carried out according to previous investigations[16,28,29] with slight modification. NOP (5 mg) was dissolved in 1 mL of ultrapure water, added 200 μL of 0.2 mol/L MES monohydrate solution, and activated by 500 μL of 200 mg/mL N-cyclohexyl-N-[2-(4-methyl-1-oxa-4-azoniacyclohex-4-yl)ethyl]methanediimine,4-methylbenzenesulfonic acid for 2 h. After adding 1 mL of 2 mol/L imidazole, the mixture was reduced with 70 mg/mL $NaBD_4$ for 3 h. By stopping with 300 μL glacial acetic acid, the reactants were dialyzed and freeze-dried. The freeze-dried products (1 mg) were dissolved in 1 mL of dimethyl sulfoxide, added 30 mg of NaOH, and incubated at room temperature for 0.5 h. With addition of 250 μL methyl iodide, the mixture was reacted under nitrogen gas in the dark for 1 h. Then, added another 250 μL methyl iodide and maintained the reaction for another 1 h. The reactants were extracted with 1 mL of distilled water and 2 mL of dichloromethane. The dichloromethane phases were collected, washed with distilled water thrice, and dried with nitrogen gas. After that, the dried samples were reacted with 1 mL of 2 mol/L trifluoroacetic acid at 121 °C for 2 h and dried with nitrogen gas. With addition of 1 mL of 1 mol/L $NaBD_4$, the mixture was incubated at room temperature with magnetic stirring for 2.5 h, and stopped by 300 μL acetic acid. The reactants were dissolved in 2 mL of 5% (v/v) acetic

acid-methanol solution and dried with nitrogen gas for two times. Then, the dried samples were dissolved in 2 mL methanol and dried with nitrogen gas for twice. After adding 1.5 mL acetic anhydride, the samples were reacted at 100 ℃ for 2.5 h and then extracted with 2 mL of distilled water and 1 mL of dichloromethane. Finally, the dichloromethane layers were collected and determined on an Agilent 7890A-5977B GC-MS system (Agilent Technologies Corp., USA) equipped with a HP-5MS (Agilent J&W Scientific, Folsom, CA, USA) capillary column (30 m × 0.25 mm i.d., 0.25 μm film thickness). The carrier gas is high-purity helium (purity ≥ 99.999%) with a flow rate of 1.0 mL/min. The injection volume is 1 μL with split injection (the split ratio is 10: 1), the temperature of the injection port is 260 ℃, and the solvent delay is 2.2 min. Meanwhile, the GC oven was maintained at 50 ℃ for 1.0 min, programmed from 50 ℃ to 130 ℃ with a rate of 50 ℃/min, programmed from 130 ℃ to 230 ℃ with a rate of 3 ℃/min, and maintained at 230 ℃ for 2 min. On the other hand, the MS operating conditions were: electron impact ion source; electron energy of 70 eV; injection port temperature of 230 ℃; quadrupole tube temperature of 150 ℃; scanning range of 30~600 m/z.

2.3.2 1D/2D NMR spectra determinations

NOP was firstly dissolved in D_2O (with TMSP as an internal reference standard) and determined on a 600 MHz Bruker spectrometer (Brucker, Rheinstetten, Germany) at 292.9 K. After determination, ^{1}H, ^{13}C, COSY, HSQC, HMBC and NOESY spectra were acquired.

2.4 Gastroprotective activity evaluation of NOP against AGML in rats

2.4.1 Animal experimental design

After a one-week acclimation period, rats were randomly divided into three groups (6 rats per group): the normal control (NC) group, the AGML control (LC) group, and NOP pre-treatment (200 mg/kg·bw; NOP) group. The dosage of NOP was set referring to our previous study[27]. The establishment of AGML model and the experimental procedures were performed according to our previous studies[13,16]. The schematic diagram of this animal experiment design is illustrated in Fig. 1.

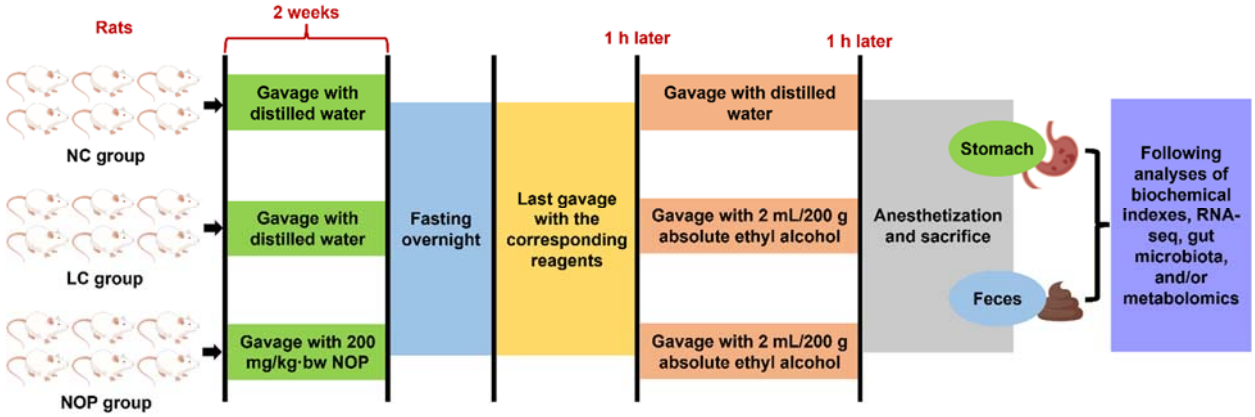

Fig. 1 The schematic diagram of animal experiment design. NC, LC and NOP represent normal control group, AGML control group, and 200 mg/kg·bw NOP pre-treatment group, respectively.

2.4.2 Gastric lesion evaluation

Stomachs of rats were opened along the greater curvature, and rinsed with precooled normal saline to remove the residues. After being blotted with filter paper and flattened, the stomachs were photographically

recorded with a digital camera. The total gastric mucosa area (TA) and total lesion area on gastric mucosa (LA) were measured by Image J, and the calculated gastric lesion area ratio (LA/TA) was used to evaluate the AGML degree[7].

Moreover, the histopathological changes of stomachs were observed using HE staining under a light microscope at 100× magnification, referring to our previous study[13].

2.4.3 Inflammation level assay

Stomach tissues were homogenized with precooled normal saline to prepare 10% homogenates. The homogenates were centrifuged (3500 rpm, 15 min) to gain the supernatants. Then, the inflammation level of the supernatants was measured using TNF-α and Il6 ELISA kits under the guide of manufacturers' instructions.

2.4.4 RNA-seq analysis of gastric tissues

Gastric tissues from three rats per group were selected for RNA-seq analysis, performed by Applied Protein Technology Co., Ltd. (Shanghai, China). Briefly, the total RNA of gastric tissues was extracted with TRIzol reagent, and the quantity and quality of obtained RNA were detected by a Nanodrop ND-2000 spectrophotometer (NanoDrop Technologies, Wilmington, USA). At the same time, RNA integrity number of obtained RNA was measured by Agilent 4150 Bioanalyzer (Agilent Technologies, Palo Alto, USA). Then, RNA-Seq library was constructed referring to the instructions of NEBNext® UltraTM RNA Library Prep Kit for Illumina®, and sequenced using a NovaSeq 6000 platform (Illumina, San Diego, USA). The quality of sequence reads was assessed by FastQC, and the FPKM value of transcription region was calculated using featureCounts software to quantify its expression abundance and variations. Principal component analysis (PCA) was performed, and differential expression analysis of genes between groups was carried out by DESeq2 software. The genes with fold change (FC) >1.0 and p-value <0.05 were considered as differentially expressed genes (DEGs), which were displayed by Volcano plot. Then, hierarchical clustering, Gene Ontology (GO) and Kyoto Encyclopedia of Genes and Genomes (KEGG) analyses for DEGs were operated. Herein, GO or KEGG items with p-value <0.05 carried out by Fisher's exact test were considered to be significantly enriched.

2.4.5 Western blot analysis of gastric tissues

Protein expressions of hub targets enriched in inflammatory signaling pathways, including Ccl2, Cxcl1, Icam1, Il6, Jun and Lif, in gastric tissues were analyzed using western blot method as previously described[13]. The distinctions were as follows: the used primary antibodies were anti-β-actin, anti-Ccl2, anti-Cxcl1, anti-Icam1, anti-Il6, anti-Jun and anti-Lif antibodies, and all dilution ratios (except anti-β-actin of 1: 10000) of them were 1: 2000; the used secondary antibody was anti-rabbit-IgG-HRP antibody, with a dilution ratio of 1: 10000 or 1: 20000.

2.4.6 Gut microbiota analysis of feces

Gut microbiota of feces was detected using 16S rRNA analysis, according to previous studies[16,30]. Briefly, DNA of feces was extracted with OMEGA Soil DNA Kit, and the 16S rRNA genes of distinct regions 16SV3-V4 were amplified. The amplified PCR products were quantified, purified, and subjected to build sequencing libraries using TruSeq Nano DNA LT Library Prep Kit. The sequencing libraries were checked, quantified, pooled and sequenced on an Illumina HiSeq platform (Applied Protein Technology Co., Ltd., Shanghai, China).

2.4.7 Untargeted metabolomics analyses of gastric tissues

Untargeted metabolomics analyses of gastric tissues were carried out by Applied Protein Technology Co., Ltd. (Shanghai, China). In brief, a part of gastric tissues was cut into pieces and ground with precooled methanol-acetonitrile-water solution (2:1:1, v/v). The homogenates were received with ultrasonication, incubation and centrifugation. Then, the gained supernatants were dried, re-dissolved, vortexed and centrifuged. Finally, the samples were detected using a UHPLC-Q-TOF/MS system, which included an Agilent 1290 Infinity LC instrument (Agilent Technologies, USA) equipped with an Acquity UPLC BEH Amide column (2.1 mm × 100 mm, 1.7 μm, Waters, Ireland) and a Triple TOF 6600 mass spectrometer (AB SCIEX, Singapore) equipped with two electrospray ionization (ESI) sources.

2.4.8 Correlation analyses among gut microbiota, metabolites and biochemical indexes

The correlations among gut microbiota, metabolites and biochemical indexes were analyzed by Spearman analysis using Origin 2022 software (OriginLab Corporation, USA) with the "Correlation Plot" package.

2.4.9 Molecular docking analysis on representative metabolites and hub targets

Molecular docking analysis on representative metabolites and hub targets were conducted as previously described[31] with modifications. Briefly, the three-dimensional (3D) structures of hub targets and the two-dimensional (2D) structures of representative metabolites were obtained, and the latter 2D structures were transformed into 3D structures. The original ligand and water in the 3D structures of hub target proteins (used as receptors) were removed, and received with hydrogen addition and charge calculation. Meanwhile, the hydrogen addition and charge calculation were performed to the 3D structures of representative metabolites (used as ligands). Then, molecular docking analyses between the receptors and the ligands were carried out using AutoDock Vina_v1.2.5 software[32,33]. Finally, the molecular docking results were visualized using LigPlus _v2.2 and PyMOL_v2.5.3 software.

2.5 Statistical analysis

All results are expressed as mean ± standard deviation (SD). Differences between all experimental groups were examined by one-way analysis of variance (ANOVA) combined with Tukey's analysis or Student's *t*-test, on a SPSS 23.0 software (Chicago, IL, USA). The p-values < 0.05 were considered statistically significant. Meanwhile, Fisher' exact test or Student's *t*-test was used for the statistical analysis of data from RNA-seq, 16S rRNA and metabolomics detections.

3. Results and discussion

3.1 Structural characteristics of NOP

In our previous work[27], chemical component, monosaccharide composition, molecular weight and Fourier transform infrared spectroscopy of NOP have been detected. In this study, the structural characteristics of NOP were further determined by methylation analysis and 1D/2D NMR spectra. As shown in Table 1, NOP contained twenty-three different glycosidic bonds, including T-Ara*f*-(1→, T-Rha*p*-(1→, →5)-Ara*f*-(1→, →2)-Rha*p*-(1→, →2)-Xyl*p*-(1→, →4)-Xyl*p*-(1→, T-Glc*p*-(1→, T-Gal*p*-(1→, T-Gal*p*A-(1→, →2,5)-Ara*f*-(1→, →2,4)-Rha*p*-(1→, →4)-Gal*p*-(1→, →4)-Gal*p*A-(1→, →2,3,5)-Ara*f*-(1→, →4)-Glc*p*-(1→, →4)-Glc*p*A-(1→, →3)-Gal*p*-(1→, →6)-Glc*p*-(1→, →6)-Gal*p*-(1→, →2,4)-Gal*p*A-(1→, →4,6)-Glc*p*-(1→, →3,6)-Glc*p*-(1→ and →3,6)-Gal*p*-(1→ residues, in a relative molar ratio of 4.62: 1.47: 5.62: 0.66: 0.39: 0.49: 0.84: 2.10: 2.98: 0.90: 0.31: 2.14: 48.37: 1.39: 1.43: 0.63: 0.75: 17.91: 1.39: 0.50: 0.67: 1.44: 2.98. The total ion chromatogram for NOP obtained by methylation analysis is shown in Fig. S1 (seen in supplementary materials), and the electron-impact mass spectra of corresponding PMAA are displayed in Fig. S2 and Fig. S3 (seen in supplementary materials). The →4)-Gal*p*A-(1→ residue had the highest ratio, indicating this residue might be within the main chain of NOP.

Table 1 Glycosidic bond types of NOP obtained by methylation analysis

RT (min)	Glycosidic bond type	Relative molar ratio (%)	Mass fragments (m/z)
11.70	T-Ara*f*-(1→	4.62	59, 71, 87, 102, 118, 129, 145, 161, 162
12.74	T-Rha*p*-(1→	1.47	59, 72, 85, 102, 118, 131, 162, 175
15.44	→5)-Ara*f*-(1→	5.62	59, 71, 87, 102, 118, 129, 162, 189
15.49	→2)-Rha*p*-(1→	0.66	59, 72, 89, 100, 118, 131, 190
15.63	→2)-Xyl*p*-(1→	0.39	59, 71, 87, 102, 118, 129, 162, 189
15.63	→4)-Xyl*p*-(1→	0.49	59, 71, 87, 102, 118, 129, 162, 189
16.77	T-Glc*p*-(1→	0.84	59, 71, 87, 102, 118, 129, 145, 161, 162, 205
17.45	T-Gal*p*-(1→	2.10	59, 71, 87, 102, 118, 129, 145, 161, 162, 205
17.45	T-Gal*p*A-(1→	2.98	59, 73, 87, 102, 118, 131, 147, 161, 162, 207
18.37	→2,5)-Ara*f*-(1→	0.90	59, 72, 87, 88, 101, 118, 130, 189, 190
18.37	→2,4)-Rha*p*-(1→	0.31	59, 72, 87, 88, 101, 118, 130, 189, 190
19.85	→4)-Gal*p*-(1→	2.14	59, 75, 87, 102, 118, 129, 162, 175, 235
19.85	→4)-Gal*p*A-(1→	48.37	59, 75, 87, 102, 118, 129, 162, 175, 235
20.01	→2,3,5)-Ara*f*-(1→	1.39	60, 73, 86, 115, 128, 145, 159, 175, 188, 201, 218, 290
20.03	→4)-Glc*p*-(1→	1.43	59, 71, 87, 99, 102, 113, 118, 129, 162, 233
20.03	→4)-Glc*p*A-(1→	0.63	59, 71, 87, 102, 113, 118, 129, 162, 233
20.31	→3)-Gal*p*-(1→	0.75	59, 71, 87, 101, 118, 129, 161, 234, 277
20.55	→6)-Glc*p*-(1→	17.91	59, 71, 87, 102, 118, 129, 162, 189, 233
21.54	→6)-Gal*p*-(1→	1.39	59, 71, 87, 99, 102, 118, 129, 162, 189, 233
22.53	→2,4)-Gal*p*A-(1→	0.50	59, 72, 88, 101, 115, 130, 190, 235
23.31	→4,6)-Glc*p*-(1→	0.67	59, 71, 85, 99, 102, 118, 127, 261
23.48	→3,6)-Glc*p*-(1→	1.44	59, 74, 87, 102, 118, 129, 160, 189, 234, 305
24.34	→3,6)-Gal*p*-(1→	2.98	59, 74, 87, 101, 118, 129, 160, 189, 234, 305

By 1D/2D NMR spectra determinations, the ^{1}H, ^{13}C, HSQC, COSY, HMBC and NOESY spectrums were obtained, as illustrated in Fig. 2(A)~2(F). In the ^{1}H NMR spectrum (Fig. 2(A)), multiple anomeric proton signals (H-1) were distributed at δ 4.3~5.5 ppm, and the proton signals of H-2~H-6 were stacked at δ 3.0~4.3

ppm, which overlapped with each other seriously and were difficult to be affiliated. Meanwhile, multiple anomeric carbon signals (C-1) were observed at δ 90~110 ppm in the ^{13}C NMR spectrum (Fig. 2(B)). Moreover, some characteristic signals could be seen from Fig. 2(A) and Fig. 2(B): the signal at high-field region of δ 1.10~1.30 ppm in the ^{1}H NMR spectrum was ascertained as the chemical shifts of H-6 for Rha*p*, and the corresponding signal at δ 17.86 ppm in the ^{13}C NMR spectrum was attributed to be the -CH_3 of Rha*p*[34]; the signals near at δ 175.96 ppm and δ 171.82 ppm in the ^{13}C NMR spectrum were respectively assigned to the C-6 of unesterified and esterified Gal*p*A[35]. With combination analyses on the ^{1}H, ^{13}C, HSQC and COSY spectra (Fig. 2(A)~2(D)) along with the ^{1}H spectrum obtained after water peak compression (Fig. S4 seen in supplementary materials), the anomeric chemical shifts (H-1 and C-1) were designated as $GE_{1,4}$ (δ 4.82, δ 101.49), $GA_{1,4}$ (δ 4.92, δ 101.33), GA_t (δ 4.91, δ 101.32), $G_{1,4}$ (δ 4.50, δ 105.52), $G_{1,3,6}$ (δ 4.34, δ 104.71), G_t (δ 4.50, δ 105.42), $Rha_{1,2}$ (δ 5.15, δ 101.89), $Rha_{1,2,4}$ (δ 5.15, δ 101.89), A_t (δ 5.11, δ 110.35), $A_{1,5}$ (δ 4.95, δ 108.74), $Glc_{1,4}$ (δ 5.27, δ 100.85) and $Glc_{1,6}$ (δ 4.50, δ 105.68). Meanwhile, all of the ^{1}H and ^{13}C chemical shifts were identified and listed in the Table 2. On the basis of previous references and the data of monosaccharide composition[27] and methylation analyses (Table 1), these residues were inferred to be $GE_{1,4}$ (→4)-α-D-6-OMe-Gal*p*A-(1→)[36], $GA_{1,4}$ (→4)-α-D-Gal*p*A-(1→)[37], GA_t (α-D-Gal*p*A-(1→)[37], $G_{1,4}$ (→4)-β-D-Gal*p*-(1→)[38], $G_{1,3,6}$ (→3,6)-β-D-Gal*p*-(1→)[36], G_t (β-D-Gal*p*-(1→)[36], $Rha_{1,2}$ (→2)-α-L-Rha*p*-(1→)[39], $Rha_{1,2,4}$ (→2,4)-α-L-Rha*p*-(1→)[40], A_t (α-L-Ara*f*-(1→)[41], $A_{1,5}$ (→5)-α-L-Ara*f*-(1→)[42], $Glc_{1,4}$ (→4)-α-D-Glc*p*-(1→)[42] and $Glc_{1,6}$ (→6)-β-D-Glc*p*-(1→)[43]. Otherwise, the ^{1}H and ^{13}C chemical shifts of other sugar residues including T-Rha*p*-(1→, →2)-Xyl*p*-(1→, →4)-Xyl*p*-(1→, T-Glc*p*-(1→, →2,5)-Ara*f*-(1→, →2,3,5)-Ara*f*-(1→, →4)-α-D-Glc*p*A-(1→, →3)-Gal*p*-(1→, →6)-Gal*p*-(1→, →2,4)-Gal*p*A-(1→, →4,6)-Glc*p*-(1→ and →3,6)-Glc*p*-(1→ were difficult to be assigned as it showed very weak signals in the NMR spectra.

Table 2 ^{1}H and ^{13}C NMR chemical shifts of each sugar residues in NOP.

Sugar residues		Chemical shifts (δ, ppm)							
			1	2	3	4	5	6	-OMe
GE1,4	→4)-α-D-GalpA-6-OMe-(1→	H	4.82	3.58	3.86	4.31	5.01	-	3.66
		C	101.49	68.93	69.42	80.38	71.68	171.82	54.12
GA1,4	→4)-α-D-GalpA-(1→	H	4.92	3.60	3.85	4.29	4.62	-	-
		C	101.33	68.92	69.75	80.22	72.17	175.96	-
GAt	α-D-GalpA-(1→	H	4.91	3.56	-	-	-	-	-
		C	101.32	69.38	-	-	-	176.94	-
G1,4	→4)-β-D-Galp-(1→	H	4.50	3.55	3.64	4.03	3.59	3.63	3.73
		C	105.52	73.13	74.58	78.82	75.70	61.75	-
G1,3,6	→3,6)-β-D-Galp-(1→	H	4.34	3.39	3.77	-	-	3.66/3.82	-
		C	104.71	72.32	82.34	-	-	67.81	-
Gt	β-D-Galp-(1→	H	4.50	3.53	3.58	3.85	3.60	3.63	3.70
		C	105.42	73.03	73.08	69.67	74.43	61.75	-
Rha1,2	→2)-α-L-Rhap-(1→	H	5.15	4.12	3.81	3.27	3.64	1.12	-
		C	101.89	78.93	71.52	70.71	69.10	17.86	-
Rha1,2,4	→2,4)-α-L-Rhap-(1→	H	5.15	4.12	3.75	3.60	3.75	1.12	-
		C	101.89	78.93	69.91	81.33	69.75	17.86	-
At	α-L-Araf-(1→	H	5.11	4.07	3.81	3.95	3.68	3.58	-
		C	110.35	82.31	77.80	82.31	62.17	-	-
A1,5	→5)-α-L-Araf-(1→	H	4.95	4.00	3.88	4.07	3.66	-	-

		C	108.74	81.90	77.67	83.58	67.81	-	-
Glc1,4	→4)-α-D-Glcp-(1→	H	5.27	3.50	3.82	3.58	3.76	3.65	-
		C	100.85	71.06	74.43	75.70	69.79	61.75	-
Glc1,6	→6)-β-D-Glcp-(1→	H	4.50	3.54	3.71	3.67	3.82	4.06	
		C	105.68	72.97	77.67	69.09	74.59	69.50	

The coupling signals of anomeric protons and carbons, anomeric carbons and protons, or protons and protons among glycosyl residues obtained from HMBC (Fig. 2(E)) and NOESY (Fig. 2(F)) spectrums, were further analyzed to identify the order of connection for the above-mentioned residues. In the HMBC (Fig. 2(E)) spectrum, coupling signals were seen between H-1 (δ 4.92) of residue $GA_{1,4}$ and C-2 (δ 78.93) of residue $Rha_{1,2}$, indicating that $GA_{1,4}$ was connected to $Rha_{1,2}$ as →4)-α-D-Gal*p*A-(1→2)-α-L-Rha*p*-(1→; cross-peaks were observed between H-1 (δ 4.95) of residue $A_{1,5}$ and C-5 (δ 67.81) of it, implying that $A_{1,5}$ was linked with itself as →5)-α-L-Ara*f*-(1→5)-α-L-Ara*f*-(1→; coupling signals were found between H-1 (δ 5.11) of residue A_t and C-3 (δ 82.34) of residue $G_{1,3,6}$, suggesting that A_t was connected to $G_{1,3,6}$ as α-L-Ara*f*-(1→3,6)-β-D-Gal*p*-(1→. Regarding the NOESY (Fig. 2(F)) spectrum, H-1 (δ 4.82) of residue $GE_{1,4}$ had cross-peaks with its H-4 (δ 4.31), showing $GE_{1,4}$ was connected to itself as →4)-α-D-Gal*p*A-6-OMe-(1→4)-α-D-Gal*p*A-6-OMe-(1→; H-1 (δ 4.50) of residue G_t showed coupling signals with its H-4 (δ 4.03), suggesting that G_t was linked with $G_{1,4}$ as β-D-Gal*p*-(1→4)-β-D-Gal*p*-(1→; coupling signals were seen between H-1 (δ 4.34) of residue $G_{1,3,6}$ and H-4 (δ 3.60) of residue $Rha_{1,2,4}$, implying that $G_{1,3,6}$ was connected to $Rha_{1,2,4}$ as →3,6)-β-D-Gal*p*-(1→2,4)-α-L-Rha*p*-(1→; H-1 (δ 4.95) of residue $A_{1,5}$ possessed cross-peaks with H-4 (δ 3.60) of $Rha_{1,2,4}$, indicating the presence of →5)-α-L-Ara*f*-(1→2,4)-α-L-Rha*p*-(1→; H-1 (δ 4.50) of residue $G_{1,4}$ exhibited coupling signals with H-4 (δ 3.60) of $Rha_{1,2,4}$, implying that $G_{1,4}$ was connected to $Rha_{1,2,4}$ as →4)-β-D-Gal*p*-(1→2,4)-α-L-Rha*p*-(1→; cross-peaks were observed between H-1 (δ 4.50) of residue $Glc_{1,6}$ and H-6 (δ 4.06) of residue $Glc_{1,6}$, suggesting $Glc_{1,6}$ was linked with itself as →6)-β-D-Glc*p*-(1→6)-β-D-Glc*p*-(1→.

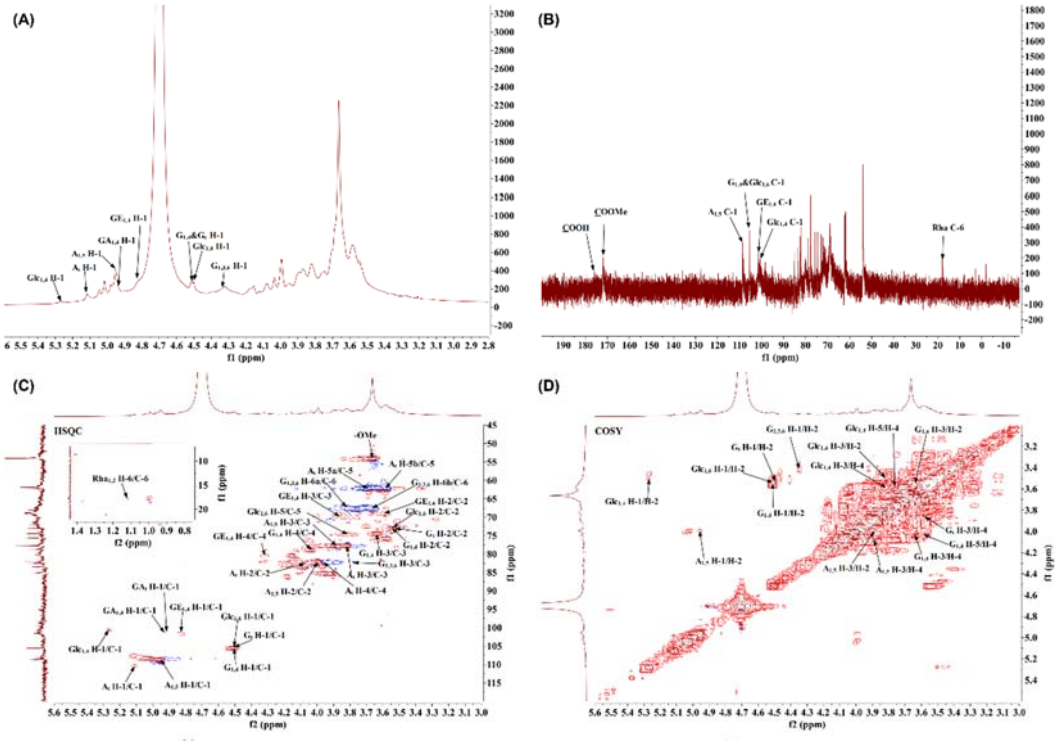

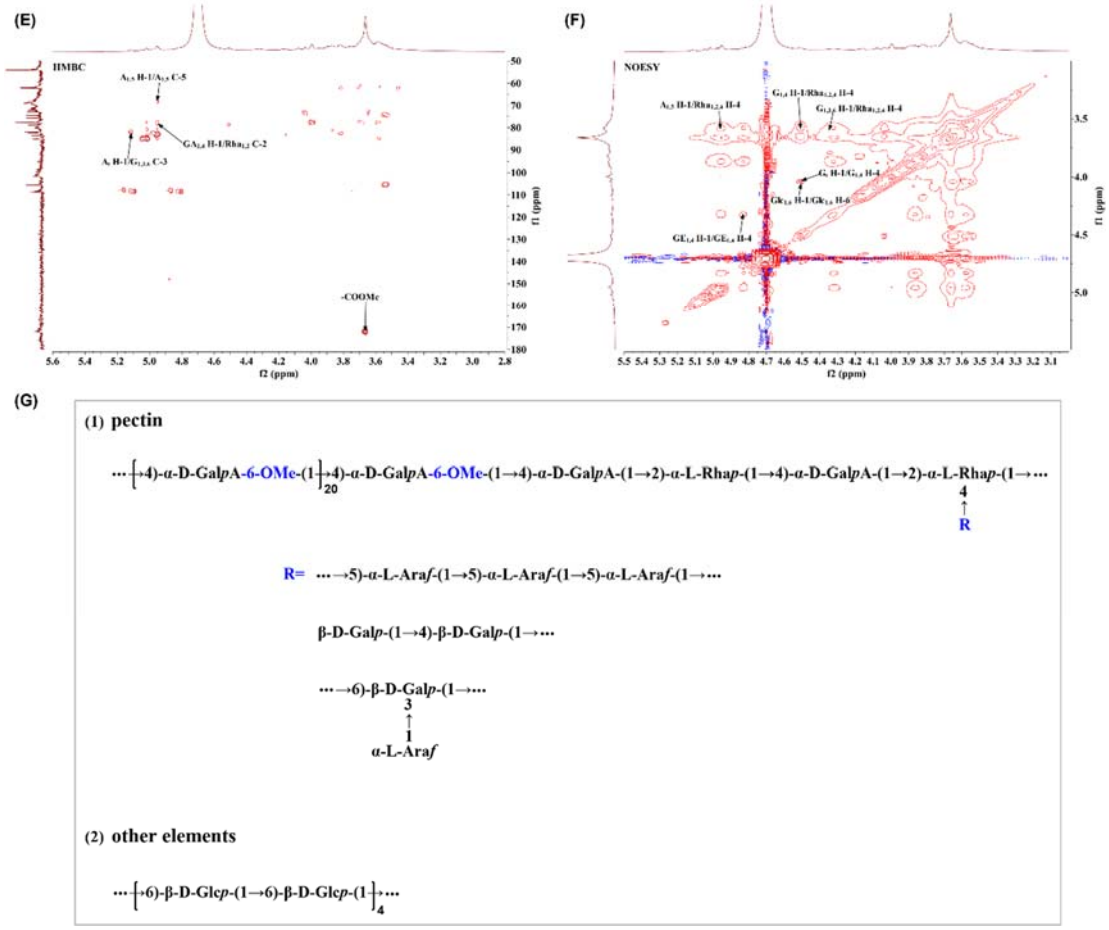

Fig. 2 1D/2D NMR spectra and possible primary structure units of NOP. (A), ^{1}H spectrum; (B), ^{13}C spectrum; (C), HSQC spectrum; (D), COSY spectrum; (E), HMBC spectrum; (F), NOESY spectrum; (G), possible primary structure units.

Based on the results of monosaccharide composition, methylation and 1D/2D NMR analyses, NOP was a complex polysaccharide and was identified to be composed of HG domain, RG-I domain and β-1,6-D-glucan structure. The side chains of RG-I domain were composed of →5)-α-L-Ara*f*-(1→, β-D-Gal*p*-(1→, →4)-β-D-Gal*p*-(1→ and →3,6)-β-D-Gal*p*-(1→ residues. Finally, the primary structure of the repeating units in NOP was predicted, as shown in Fig. 2(G).

3.2 Effects of NOP on AGML and inflammation level of rats

Alcohol can induce obvious bleeding strips on the gastric mucosal surfaces[13,16]. Several pectic polysaccharides from *Sedum dendroideum*[25], *Evodiae fructus*[16], *Artemisia campestris subsp maritima*[24], *Croton cajucara*[26] and *Prunus domestica*[23] have been demonstrated to ameliorate AGML in mice or rats. As shown in Fig. 3(A), rats in the LC and NOP groups showed obvious bleeding strips on the gastric mucosal surfaces, whereas no such indications were observed in the NC group. Compared with the NC group, many serious and significant bleeding strips were observed on the gastric mucosa of rats in the LC group. However, the bleeding strips on the gastric mucosa of rats in the NOP group were markedly fewer than those in the LC group. Moreover, the gastric lesion area ratio was dramatically lower in the NOP group compared to the LC group, as illustrated in Fig. 3(C). Meanwhile, HE staining revealed remarkable losses of gastric glandular structure in the LC group compared to the NC group (Fig. 3(B)). Compared with the LC group, this

phenomenon was observably alleviated in the NOP group. These results indicated that 200 mg/kg·bw NOP pre-treatment could ameliorate AGML in rats.

Excess alcohol has been demonstrated to trigger the inflammatory response in gastric tissue, which might then lead to secondary mucosal damage[44,45]. TNF-α and Il6 are two main pro-inflammatory cytokines. In the Fig. 3(D) and Fig. 3(E), the levels of TNF-α and Il6 in gastric tissues of rats were dramatically increased in the LC and NOP groups, as compared with the NC group. This revealed that alcohol induced inflammatory responses to gastric tissues of rats. Compared with the LC group, these two indexes were significantly decreased in the NOP group, indicating 200 mg/kg·bw NOP pre-treatment could lower inflammatory responses in the gastric tissues of AGML rats. In the previous studies, polysaccharides from *Dendrobium huoshanense* stem[7], purple sweet potato[46], *Dendrobium officinale*[9], *Lacticaseibacillus rhamnosus*[47] have also been proven to reduce inflammatory responses in the gastric tissues of AGML rats.

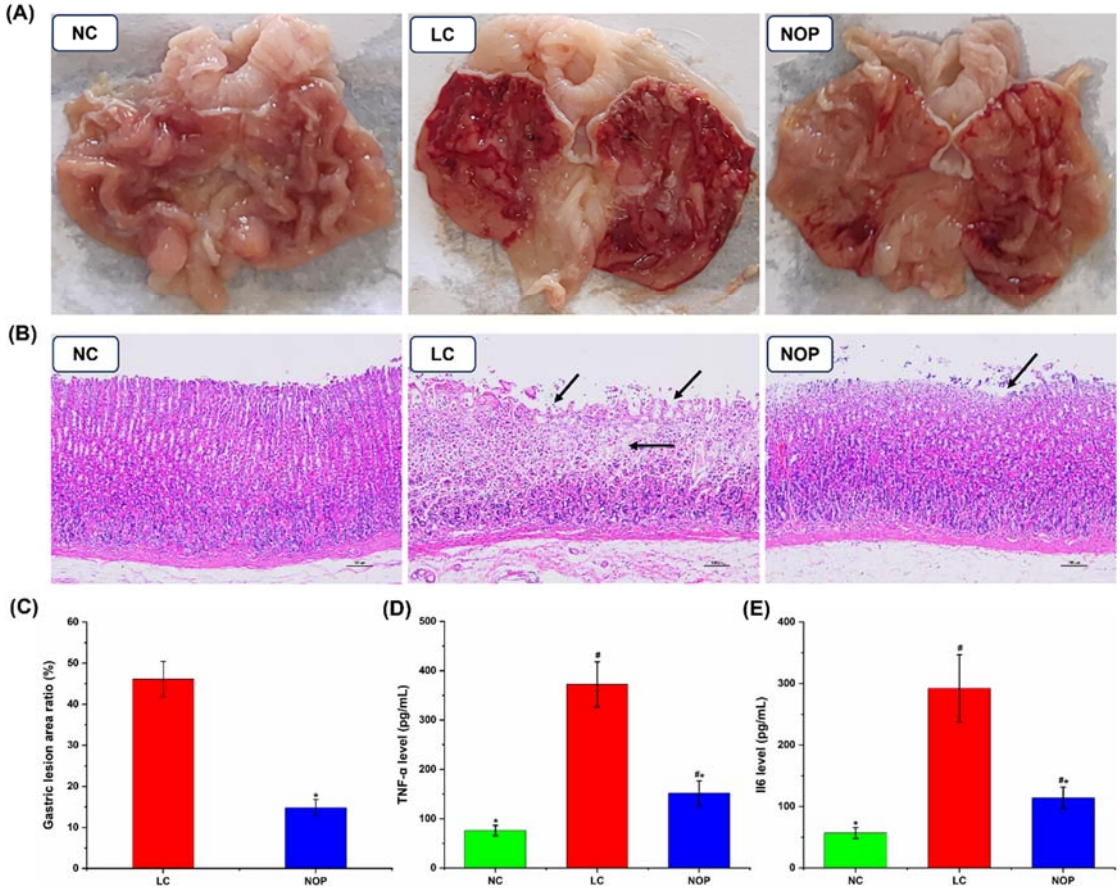

Fig. 3 Effects of NOP on AGML and inflammation level of rats (n=6). (A), macroscopic observation of stomachs; (B), HE staining of gastric tissues (arrows represent stomach glandular structure loss); (C), gastric lesion area ratio; (D), TNF-α level; (E), Il6 level. In the Fig. 3(C) ~ 3(E), * indicates a significant difference compared to LC group ($P < 0.05$), and # indicates a significant difference compared to NC group ($P < 0.05$). NC, LC and NOP represent normal control group, AGML control group, and 200 mg/kg·bw NOP pre-treatment group, respectively.

3.3 Gene expression changes of NOP on gastric tissues of AGML rats

Gene expression changes of NOP on gastric tissues of AGML rats are displayed in Fig. 4. As shown in PCA score plot (Fig. 4(A)), RNA samples of gastric tissues among NC, LC and NOP groups were relatively separated. The volcano plots (Fig. 4(B) and Fig. 4(C)) reveal that many significantly up- or down-regulated

genes were identified in LC group vs NC group and in NOP group vs LC group. In the Fig. 4(D), 1323, 219 and 408 DEGs were seen in LC group vs NC group, NOP group vs LC group and NOP group vs NC group, successively. Meanwhile, 181 common DEGs were screened from LC group vs NC group and NOP group vs LC group. The information and change trends of these 181 common DEGs are summarized in Table S1 (seen in supplementary materials). These results showed that 200 mg/kg·bw NOP pre-treatment generated significant changes to gene expressions in gastric tissues of AGML rats. With GO analysis on DEGs of LC group vs NC group, 742 cellular components (CC), 1363 molecular functions (MF) and 7709 biological processes (BP) items were enriched. Regarding GO analysis on DEGs of NOP group vs LC group, 348 CC, 560 MF and 3785 BP items were enriched. Each top 10 items of them are illustrated in Fig. 4(E) and Fig. 4(F), respectively. Regarding LC group vs NC group, the top 10 BP items were response to stimulus, multicellular organismal process, regulation of multicellular organismal process, response to external stimulus, regulation of multicellular organismal development, inflammatory response, etc. Whilst, in terms of NOP group vs LC group, the top 10 BP items were response to stimulus, response to bacterium, response to wounding, wound healing, immune system process, oxygen transport, inflammatory response, etc. It could be found that the inflammatory response item was enriched in both LC group vs NC group and NOP group vs LC group, further confirming regulation of inflammatory response was an important way for NOP ameliorating AGML in rats.

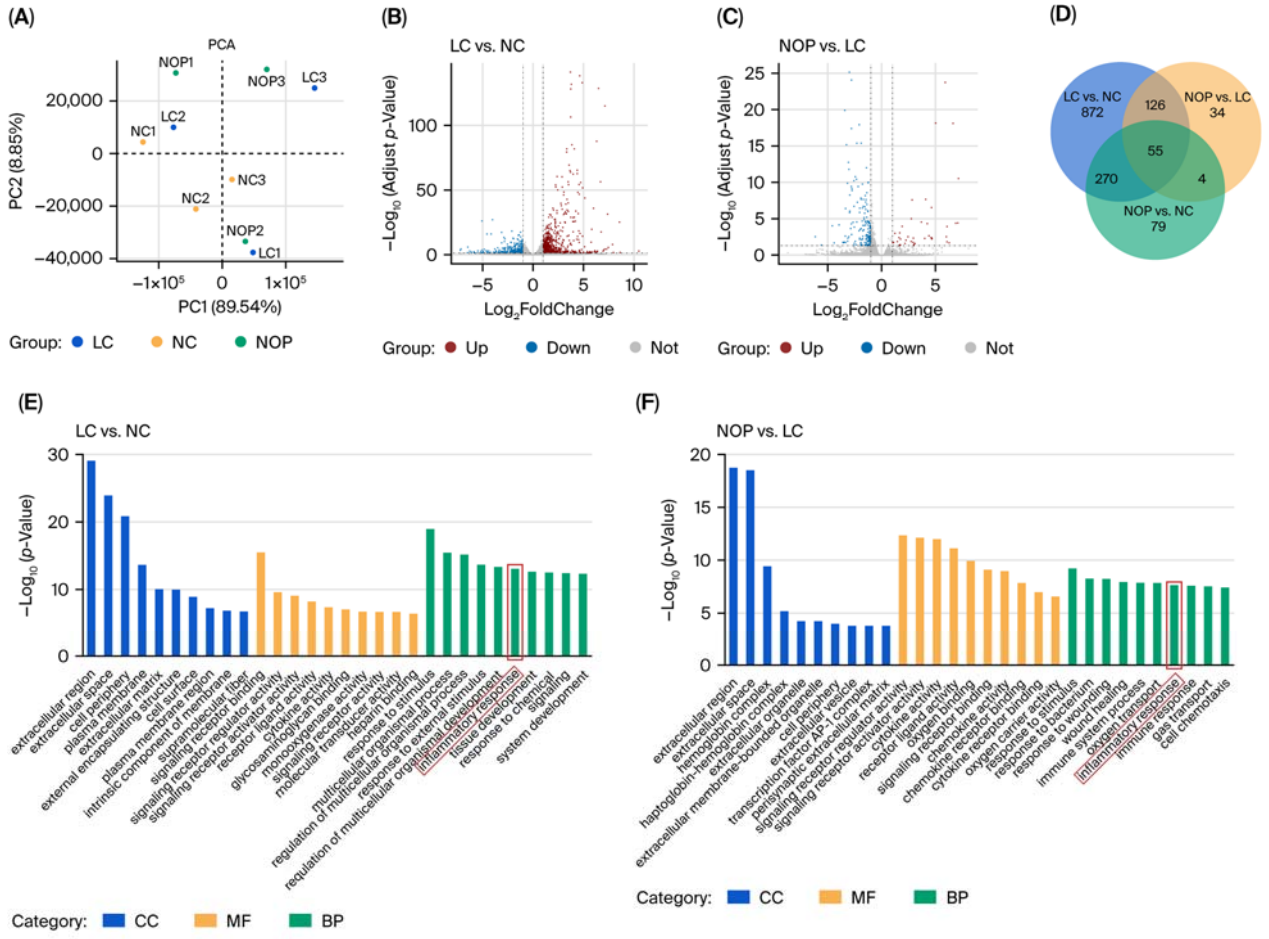

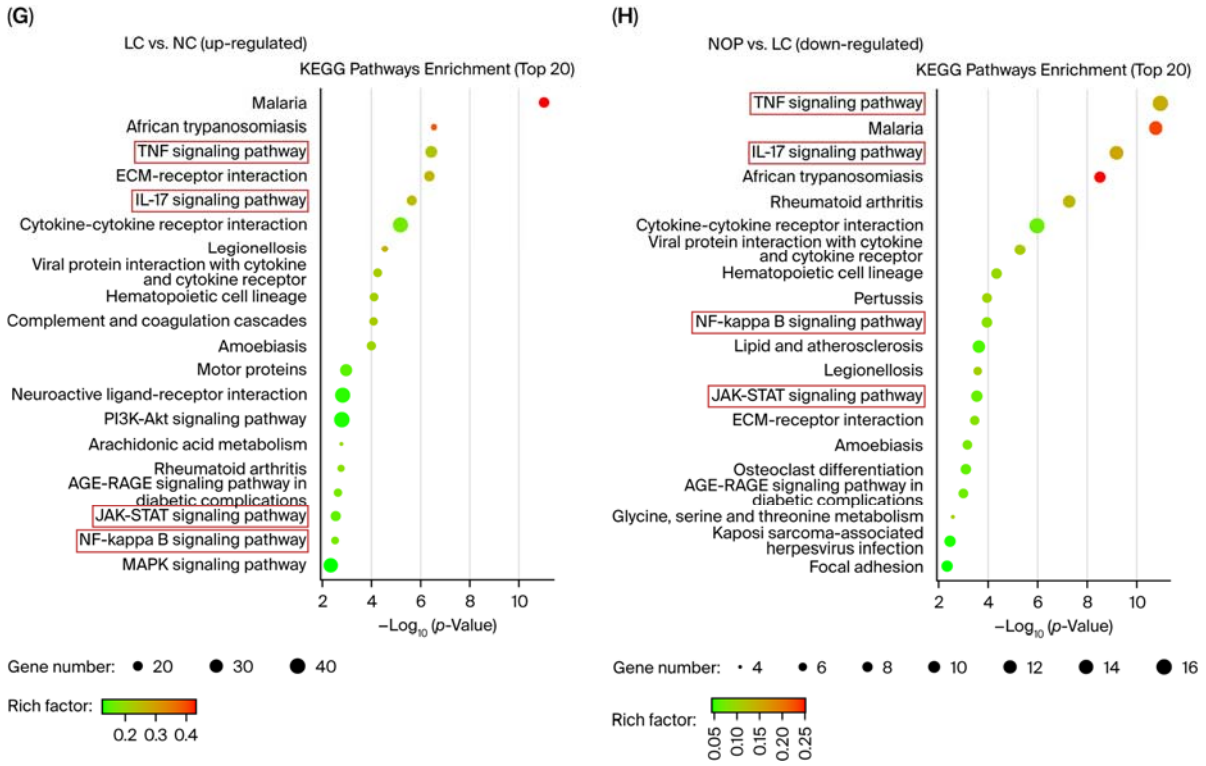

Fig. 4 Gene expression changes of NOP on gastric tissues of AGML rats obtained by RNA-seq analysis (n=3). (A), PCA score plot of gastric tissues among NC, LC and NOP groups; (B), Volcano plot of genes in LC vs NC group; (C), Volcano plot of genes in NOP vs LC group; (D), Venn diagram showing shared and unique DEGs among LC vs NC, NOP vs LC and NOP vs NC groups; (E), top 30 significant GO terms of DEGs in LC vs NC group; (F), top 30 significant GO terms of DEGs in NOP vs LC group; (G), top 20 significant up-regulated KEGG pathways of DEGs in LC vs NC group; (H), top 20 significant down-regulated KEGG pathways of DEGs in NOP vs LC group. NC, LC and NOP represent normal control group, AGML control group, and 200 mg/kg·bw NOP pre-treatment group, respectively.

By KEGG pathway analyses on DEGs, 22 down-regulated and 48 up-regulated pathways were enriched in LC group vs NC group, whilst 40 down-regulated and 12 up-regulated pathways were involved in NOP group vs LC group. Thereinto, the top 20 up-regulated or down-regulated pathways are shown in Fig. 4(G) and Fig. 4(H). Among them, 14 pathways including malaria, TNF signaling pathway, cytokine-cytokine receptor interaction, IL-17 signaling pathway, african trypanosomiasis, amoebiasis, ECM-receptor interaction, viral protein interaction with cytokine and cytokine receptor, hematopoietic cell lineage, legionellosis, NF-kappa B (NF-κB) signaling pathway, JAK-STAT signaling pathway, AGE-RAGE signaling pathway in diabetic complications and rheumatoid arthritis were respectively up-regulated in LC group vs NC group (Fig. 4(G)) and down-regulated in NOP group vs LC group (Fig. 4(H)). Among them, TNF signaling pathway, IL-17 signaling pathway, NF-κB signaling pathway and JAK-STAT signaling pathway are well-known inflammatory signaling pathways. Gene set enrichment analysis (GESA) analyses (seen in Fig. S5 in supplementary materials) further showed that these four signaling pathways were significantly down-regulated in NOP group vs LC group. Previous studies have reported that acute excessive alcohol exposure activates these four signaling pathways in gastric tissues[6,44,48]. Whilst, polysaccharides from *Panax ginseng*[6] and *Sargassum siliquastrum*[44] have been demonstrated to down-regulate NF-κB and JAK-STAT signaling pathways in gastric tissues of AGML rats. However, the present study is the first to find that

polysaccharide treatment down-regulates the TNF and IL-17 signaling pathways in gastric tissues of AGML rats.

3.4 Effects of NOP on hub targets of TNF, IL-17, NF-κB and JAK-STAT signaling pathways in gastric tissues of AGML rats

Based on above results, TNF, IL-17, NF-κB and JAK-STAT signaling pathways were selected for further analyses and determinations. The protein-protein interaction networks for DEGs enriched in these four pathways were constructed and visualized, as illustrated in Fig. 5(A)~Fig. 5(D). By topological analyses, the hub genes were screened out according to the values of network density, network centralization, network heterogeneity, and characteristic path length[31]: Cxcl1, Ccl2, Il6 and Jun for TNF signaling pathway; Il6, Ccl2 and Jun for IL-17 signaling pathway; Icam1 and Cxcl1 for NF-κB signaling pathway; Il6 and Lif for JAK-STAT signaling pathway. Thereinto, Cxcl1 has been reported to secret at high levels by the gastric epithelium at steady state, and be up-regulated during *Helicobacter pylori* infection[49]. Ccl2 recruits macrophages to inflammatory sites during tissue damage or infection[50]. Il6 and Lif are essential in the pathophysiology of multiple gastrointestinal disorders[51]. Jun has also been screened to be one of hub genes for the development and restoration of stress-induced gastric ulcer[52]. Icam1 expression is greatly elevated at sites of inflammation, thereby regulates cell-cell interactions and inflammatory responses[53]. Accordingly, Ccl2, Cxcl1, Icam1, Il6, Jun and Lif could be considered as the hub targets for NOP in regulating inflammatory signaling pathways to reduce inflammatory responses in the gastric tissues of AGML rats.

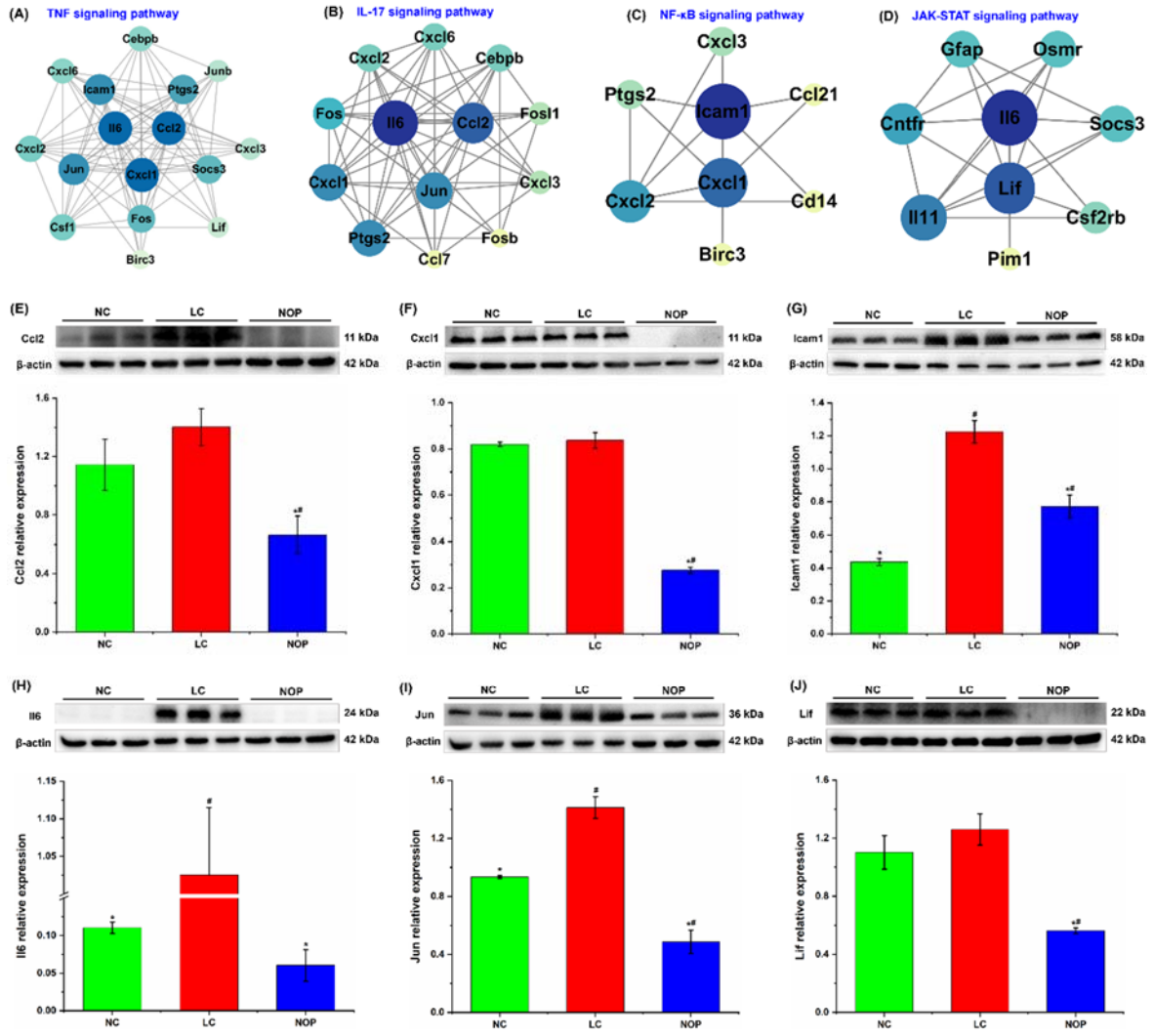

Fig. 5 Hub targets screening and their western blot validation. (A)~(D), hub targets screening from DEGs which enriched in TNF, IL-17, NF-κB and JAK-STAT signaling pathways, successively; (E)~(J) western blot analyses on protein expressions of hub targets including Ccl2, Cxcl1, Icam1, Il6, Jun and Lif, successively (n=6). In the Fig. 5(E)~5(J), * indicates a significant difference compared to LC group ($P < 0.05$), and $^{\#}$ indicates a significant difference compared to NC group ($P < 0.05$). NC, LC and NOP represent normal control group, AGML control group, and 200 mg/kg·bw NOP pre-treatment group, respectively.

The effects of NOP on the protein expressions of these six hub targets are shown in Fig. 5(E)~Fig. 5(J). The protein expressions of Icam1, Il6 and Jun in gastric tissues of rats were significantly increased, whereas those of Ccl2, Cxcl1 and Lif were not notably changed in the LC group, as compared with the NC group. Meanwhile, compared with the NC group, the protein expressions of Ccl2, Cxcl1, Jun and Lif were markedly decreased and that of Icam1 was dramatically elevated, whilst that of Il6 was not observably altered in the NOP group. Moreover, as in comparison with the LC group, the protein expressions of Ccl2, Cxcl1, Icam1, Il6, Jun and Lif were significantly declined in the NOP group. In the previous studies, polysaccharides from *Lycium barbarum*[54] and *Aureobasidium Pullulans* culture medium[55] have been indicated to reduce the level or expression of Icam1 in gastric tissues of AGML rats or mice. Polysaccharide from *Dendrobium officinale* has been demonstrated to lower the protein expression of Il6 in gastric tissues of AGML rats[56]. However, in this study, we report for the first time that polysaccharide administration reduced the expressions of Ccl2, Cxcl1, Jun and Lif in gastric tissues of AGML rats.

3.5 Metabolism changes of NOP on gastric tissues of AGML rats

Polysaccharides from *Evodiae fructus*[13,16] and *Dendrobium flexicaule*[57] have been shown to markedly change serum or liver metabolism of AGML rats or mice. The effects of NOP on gastric tissue metabolism of AGML rats are displayed in Fig. 6(A)~Fig. 6(H). In the Fig. 6(A) and Fig. 6(B), gastric tissue samples among NC, LC and NOP groups were relatively separated under ESI+ and ESI- modes in the PCA score plots, respectively. The volcano plots (Fig. 6(C)~Fig. 6(F)) show many significantly up- or down-regulated metabolites were identified in LC group vs NC group and in NOP group vs LC group under ESI+ and ESI- modes. In terms of LC group vs NC group, 75 differential metabolites (27 up-regulated and 48 down-regulated) were determined under ESI+ mode (Fig. 6(C)), and 98 differential metabolites (29 up-regulated and 69 down-regulated) were screened under ESI- mode (Fig. 6(D)). Regarding NOP group vs LC group, 24 differential metabolites (16 up-regulated and 8 down-regulated) were detected under ESI+ mode (Fig. 6(E)), and 22 differential metabolites (10 up-regulated and 12 down-regulated) were ascertained under ESI- mode (Fig. 6(F)). These metabolites mainly belonged to five classes: lipids and lipid-like molecules; organic acids and derivatives; organic nitrogen compounds; organic oxygen compounds; and organoheterocyclic compounds. Moreover, a total of 32 common differential metabolites (N-stearoylsphinganine, PC(16:0/16:0), glycerophosphocholine, prostaglandin a2, timosaponin b ii, etc.) in gastric tissues of rats were filtrated between LC group vs NC group and NOP group vs LC group, as listed in Table 3. These 32 common differential metabolites might be the potential metabolic biomarkers for the protective effect of NOP against AGML in rats. Apart from 1,2-dioleoyl-sn-glycero-3-phosphoethanolamine, the remaining 31 differential metabolites exhibited different trends (up or down) between LC group vs NC group and NOP group vs LC group. Among them, betaine, carnitine and phosphocholine have been proven to exert gastroprotective capability against ethanol or HCl/ethanol-induced gastric mucosal injury in rats[58-60]. Glycerophosphocholine, uridine and ethyl glucuronide have been screened to be three of potential metabolic biomarkers for polysaccharide from *Evodiae fructus* in mitigating AGML in mice[13]. Deoxycytidine has been determined to be one of potential metabolic biomarkers for polysaccharide from small black soybean in ameliorating acetic acid-induced gastric ulcer in rats[11]. PC(16:0/16:0), 11s-Hydroxy-5z,8z,12e,14z-eicosatetraenoic acid and L-threonine have been respectively identified to be one of potential metabolic biomarkers for dehydroevodiamine from *Evodiae fructus*[61], *Camellia* oil[62] and Zuojin Pill[63] in alleviating chronic atrophic gastritis or AGML in rats or mice.

By KEGG analyses on the obtained differential metabolites, 35 and 17 significant metabolic pathways were respectively enriched for LC group vs NC group and NOP group vs LC group. The top 20 significant metabolic pathways for LC group vs NC group and all of the significant metabolic pathways for NOP group vs LC group were respectively revealed in Fig. 6(G) and Fig. 6(H). There were nine common significant metabolic pathways (choline metabolism in cancer; central carbon metabolism in cancer; protein digestion and absorption; mineral absorption; aminoacyl-tRNA biosynthesis; ABC transporters; glycerophospholipid metabolism; biosynthesis of amino acids; and glycine, serine and threonine metabolism) between LC group vs

NC group and NOP group vs LC group. This indicated that NOP could attenuate AGML in rats through altering these nine significant metabolic pathways. Thereinto, the refined polysaccharide from *Evodiae fructus* has been indicated to modulate the metabolic pathway of choline metabolism in cancer in the liver tissues of AGML mice[13]. The polysaccharide from *Dendrobium flexicaule* has been demonstrated to regulate the metabolic pathways of choline metabolism in cancer and glycerophospholipid metabolism in the serum of AGML rats[57]. The purified pectic fraction of refined polysaccharide from *Evodiae fructus* has been determined to alter the remaining seven common significant metabolic pathways in the serum of AGML rats[16].

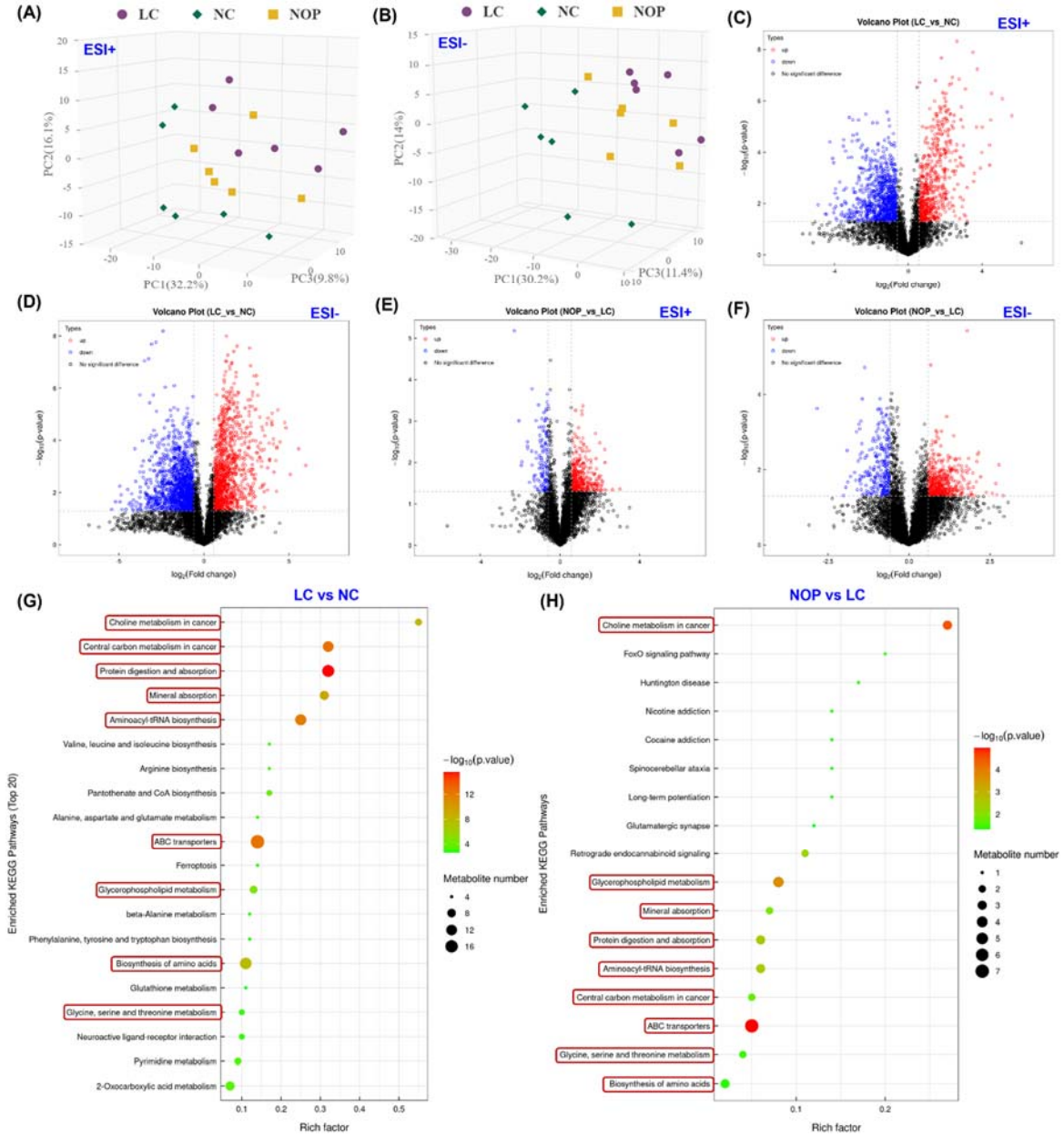

Fig. 6 Metabolism changes of NOP on gastric tissues of rats obtained by untargeted metabolomics analysis (n=6). (A) and (B), PCA score plots of gastric tissues among NC, LC and NOP groups respectively in ESI+ and ESI- modes; (C) and (D), volcano plots of differential metabolites between LC vs NC group respectively in ESI+ and ESI- modes; (E) and (F), volcano plots of differential metabolites between NOP vs LC group respectively in ESI+ and ESI- modes; (G), top 20 significant enriched KEGG pathways of differential metabolites in LC vs NC group; (H), significant enriched KEGG pathways of differential metabolites in NOP vs LC group. NC, LC and NOP represent normal control group, AGML control group, and 200 mg/kg·bw NOP pre-treatment group, respectively.

Table 3 Common differential metabolites in gastric tissues of rats between LC vs NC and NOP vs LC groups

Number	RT (min)	Detected m/z	Adduct	Identified metabolites	Trend	
					LC vs NC	NOP vs LC
In ESI+ model						
1	0.59	568.56	[M+H]+	N-stearoylsphinganine	↓	↑
2	0.69	744.55	[M+H]+	1,2-Dioleoyl-sn-glycero-3-phosphoethanolamine	↓	↓
3	2.59	734.57	[M+H]+	PC(16:0/16:0)	↓	↑
4	6.69	258.11	[M+H]+	Glycerophosphocholine	↓	↑
5	0.96	327.22	[M+H-H2O]+	13-Hydroxy-4z,7z,10z,14e,16z,19z-Docosahexaenoic acid	↑	↓
6	3.70	228.10	[M+H]+	Deoxycytidine	↑	↓
7	3.71	455.17	[2M+H]+	2'-Deoxycytidine	↑	↓
8	7.29	213.12	[M+H]+	Pro-pro	↓	↑
9	4.82	118.09	[M+H]+	Betaine	↓	↑
10	5.56	116.07	[M+H]+	DL-proline	↓	↑
11	6.88	148.06	[M+H]+	Glutamic acid	↓	↑
12	5.56	70.06	[M+H-2H2O]+	Diethanolamine	↓	↑
13	6.18	162.12	[M+H]+	Carnitine	↓	↑
14	8.51	184.08	[M+H]+	Phosphocholine	↓	↑
15	3.08	137.04	[M+H]+	Hypoxanthine	↓	↑
In ESI- model						
16	2.06	333.21	[M-H]-	Prostaglandin a2	↑	↓
17	2.98	919.47	[M-H]-	Timosaponin b ii	↑	↓
18	0.99	319.23	[M-H]-	11s-Hydroxy-5z,8z,12e,14z-eicosatetraenoic acid	↑	↓
19	1.82	335.22	[M-H]-	Prostaglandin a1	↑	↓
20	2.86	243.06	[M-H]-	Uridine	↓	↑
21	6.91	247.09	[M-H]-	Thr-Glu	↓	↑
22	3.00	277.15	[M-H]-	Leu-Phe	↓	↑
23	7.07	233.08	[M-H]-	Ser-Glu	↓	↑
24	4.97	244.13	[M-H]-	Asn-Leu	↓	↑
25	4.78	218.10	[M-H]-	Pantothenate	↓	↑
26	5.36	367.11	[M-H]-	Trans-3'-hydroxycotinine o-.beta.-d-glucuronide	↑	↓
27	5.43	221.07	[M-H]-	Ethyl glucuronide	↑	↓
28	4.62	637.28	[2M-H]-	Norfloxacin	↓	↑
29	4.79	181.05	[M-H]-	1-Methyluric acid	↓	↑
30	6.71	118.05	[M-H]-	L-Threonine	↓	↑
31	1.89	319.23	[M-H]-	12(R)-HETE	↑	↓
32	0.60	267.27	[M-H]-	Stearaldehyde	↑	↓

3.6 Gut microbiota regulation of NOP on feces of AGML rats

Alcohol consumption can disrupt the balance of the gut microbiota[64,65]. Polysaccharides from *Evodiae fructus*[16] and *Dendrobium officinale*[9] have been demonstrated to notably regulate gut microbiota of AGML rats. Effects of NOP on gut microbiota in the feces of AGML rats are illustrated in Fig. 7(A)~Fig. 7(I). The operational taxonomic units (OTUs) of NC, LC and NOP groups were 1543, 1571 and 1844, indicating NOP generated an increase trend in OTUs quantity. The NC and LC, LC and NOP, and NOP and NC groups shared 1095, 1190 and 1180 OTUs, respectively. At phylum level (Fig. 7(A)), the gut microbiota in the feces of rats among NC, LC and NOP groups were mainly p_Firmicutes, p_Bacteroidota, p_Patescibacteria and p_Proteobacteria, accounting for over 99%. The Firmicutes/Bacteroidota ratio of rats in the LC group was lower than that in the NC group, whereas NOP pre-treatment enlarged this ratio. This change was consistent with findings for polysaccharide from *Sarcodon aspratus* on water immersion and restraint stress-induced

gastric ulcer in rats[12], and for that from *Evodiae fructus* against AGML in rats[16]. Whilst, this trend was different from the observations for *Dendrobium officinale* polysaccharide against AGML in rats[9], and those for small black soybean polysaccharide on acetic acid-induced gastric ulcer in rats[11]. At genus level (Fig. 7(B)), NOP pre-treatment increased the abundances of *g_Lactobacillus*, *g_Clostridia_UCG-014* and *g_Streptococcus*, and decreased the amounts of *g_Muribaculaceae*, *g_Lachnospiraceae_NK4A136_group*, *g_Romboutsia*, *g_Prevotellaceae_NK3B31_group*, *g_UCG-005*, f_Lachnospiraceae|*g_uncultured*, and f_Oscillospiraceae|*g_uncultured*. Among them, *g_Lactobacillus* is generally considered to be a beneficial organism, and its administration has been demonstrated to significantly alleviate AGML in mice[66]. Polysaccharides from *Sarcodon aspratus*[12], *Evodiae fructus*[16] and *Dendrobium officinale*[9] have also been found to enhance the abundance of *g_Lactobacillus* in the feces of water immersion and restraint stress-induced gastric ulcer rats or AGML rats. Turmeric polysaccharide has been demonstrated to increase the number of *g_Clostridia_UCG-014* when ameliorating dextran sulfate sodium-induced ulcerative colitis[67]. Probiotic mixture containing *Streptococcus* species have been proven to accelerate healing of acetic acid-induced gastric ulcer in rats[68].

On the other hand, alpha diversity is a comprehensive indicator reflecting community richness and evenness[9]. The parameters of alpha diversity, including Chao1 index, ACE index, Shannon index and Simpson index are revealed in Fig. 7(C)~Fig. 7(F). No significant difference was observed in these four indexes between the NC group and the LC group. Meanwhile, no remarkable distinction was found in Shannon and Simpson indexes among NC, LC and NOP groups. The Chao1 and ACE indexes of the NOP group were obviously higher than those of the NC or LC group. Beta diversity, an indicator of differences in species communities between samples, was visualized using NMDS plots (Fig. 7(G)). The NC, LC and NOP groups exhibited commonalities in gut microbiota composition, which was evidenced by overlaps among them. Moreover, the samples of NC, LC and NOP groups appeared different separate distances, implying the gut microbiota structures of them were different. These above results revealed that NOP pre-treatment added the richness and evenness and altered the structure of AGML rats, which was similar to polysaccharides from *Evodiae fructus*[16] and *Dendrobium officinale*[9].

To further identify the specific bacterial taxa between NOP group and LC group, the LEfSe analysis was conducted (Fig. 7(H) and Fig. 7(I)). The dominant biomarker taxa between NOP group and LC group were o_Enterobacterales, o_Staphylococcales, f_Enterobacteriaceae, f_Bacteroidaceae, f_Tannerellaceae, *g_Klebsiella*, *g_Bacteroides*, *g_Rikenellaceae_RC9_gut_group* and *g_Parabacteroides*. Compared with the LC group, the abundances of o_Enterobacterales, o_Staphylococcales, f_Enterobacteriaceae and *g_Klebsiella* were markedly increased, whereas those of f_Bacteroidaceae, f_Tannerellaceae, *g_Bacteroides*, *g_Rikenellaceae_RC9_gut_group* and *g_Parabacteroides* were dramatically decreased in the NOP group. Among them, higher abundances of o_Enterobacterales and f_Enterobacteriaceae may confer protection against gastroduodenal ulcer[69]. The presence of f_Bacteroidaceae displays a higher abundance in the stomach of peptic ulcer disease patients[70]. Polysaccharide from *Sarcodon aspratus* has been demonstrated to

produce a notable reduction in the relative abundances of *g_Bacteroides* and *g_Parabacteroides* in the feces of water immersion and restraint stress-induced gastric ulcer rats[12]. *Phyllanthus emblica* polyphenols have been proven to decline the abundance of *g_Rikenellaceae_RC9_gut_group* in the feces of dextran sulfate sodium-induced ulcerative colitis mice[71].

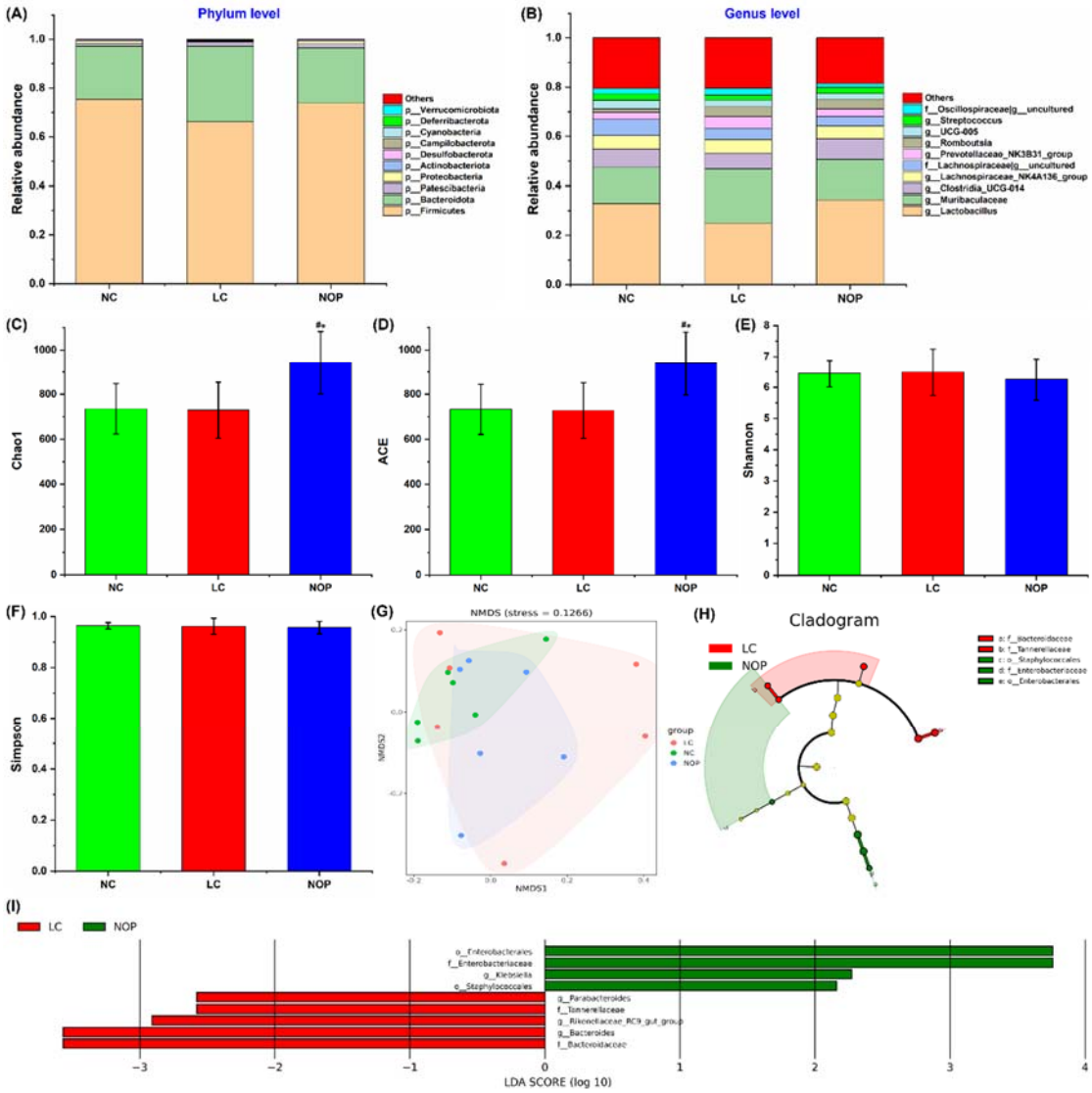

Fig. 7 Gut microbiota changes of NOP on feces of rats obtained by 16S rRNA analysis. (A) and (B), relative abundance of microbial species in the feces among NC, LC and NOP groups at phylum level and at genus level, respectively; (C)~(F), alpha diversity analyzed by Chao1, ACE, Shannon and Simpson indexes among NC, LC and NOP groups, successively; (G) NMDS plots (based on unweighted UniFrac distance) for beta diversity among NC, LC and NOP groups; (H), LEfSe analysis of taxonomic cladogram between NOP vs LC group; (I), LEfSe analysis of the dominant biomarker taxa between NOP and LC group. NC, LC and NOP represent normal control group, AGML control group, and 200 mg/kg·bw NOP pre-treatment group, respectively.

3.7 Correlations among gut microbiota biomarkers, biochemical indexes and metabolites affected by NOP

Accumulating evidence indicates that gut microbiota plays crucial roles in mediating the gastroprotective[9,11,12,16] or other activities[72-75] of polysaccharides. The relationships between gut microbiota biomarkers and biochemical indexes affected by NOP are shown in Fig. 8. f_Tannerellaceae and *g_Parabacteroides* were positively correlated with gastric lesion area ratio, TNF-α level, Il6 level, Ccl2 protein, Cxcl1 protein, Icam1 protein, Il6 protein, Jun protein and Lif protein. f_Bacteroidaceae and

g_Bacteroides showed significantly positive correlations with TNF-α level, Il6 level, Ccl2 protein, Cxcl1 protein, Icam1 protein, Jun protein and Lif protein. *g_Rikenellaceae_RC9_gut_group* was positively related to Il6 level, Ccl2 protein, Cxcl1 protein, Il6 protein, Jun protein and Lif protein. *g_Klebsiella* was negatively correlated with gastric lesion area ratio and Il6 level. These findings indicated that the gastroprotective activity of NOP on AGML in rats was related to gut microbiota regulation.

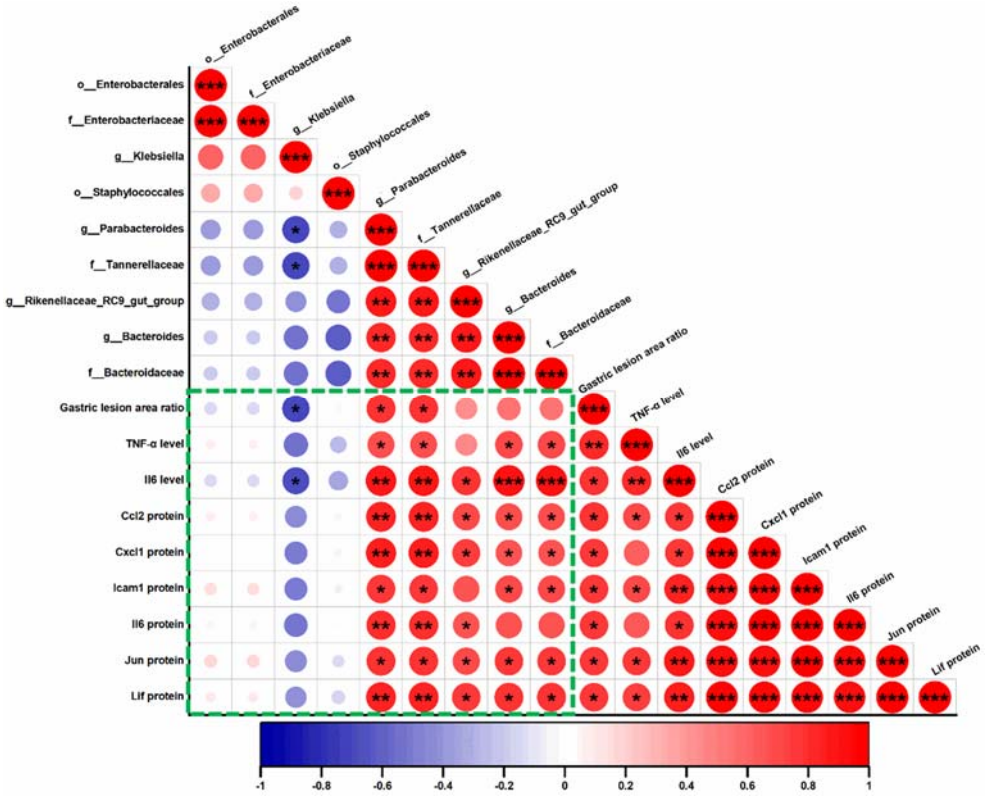

Fig. 8 Correlations between gut microbiota biomarkers and biochemical indexes of rats. $^{*}P < 0.05$, $^{**}P < 0.01$ and $^{***}P < 0.001$.

The modulation of gut microbiota metabolites is an important mechanism of interaction between polysaccharides and the gut microbiota[76]. Gut microbiota metabolites can be absorbed by intestinal epithelial cells and resident inflammatory cells, transported to various organs via systemic circulation, and thereby maintaining host health[77]. The relationships between differential metabolites and gut microbiota biomarkers affected by NOP are shown in Fig. 9. It could be seen that 13-hydroxy-4z,7z,10z,14e,16z,19z-docosahexaenoic acid, 12(R)-HETE, stearaldehyde and trans-3'-hydroxycotinine o-.beta.-d-glucuronide exhibited significantly positive correlations with f_Tannerellaceae, f_Bacteroidaceae, *g_Parabacteroides*, *g_Bacteroides* and *g_Rikenellaceae_RC9_gut_group*. Whilst, diethanolamine, DL-proline, Asn-Leu, Leu-Phe, L-threonine, pantothenate and Ser-Glu showed notably negative correlations with f_Tannerellaceae, f_Bacteroidaceae, *g_Rikenellaceae_RC9_gut_group*, *g_Parabacteroides* and *g_Bacteroides*. 2'-Deoxycytidine, deoxycytidine and 11s-hydroxy-5z,8z,12e,14z-eicosatetraenoic acid and ethyl glucuronide were positively correlated with f_Tannerellaceae and *g_Parabacteroides*. Carnitine was negatively related to f_Tannerellaceae and *g_Parabacteroides*. Prostaglandin a1 and timosaponin b ii were positively correlated with f_Tannerellaceae,

g_Parabacteroides and *g_Rikenellaceae_RC9_gut_group*. Glutamic acid and PC(16:0/16:0) were positively related to *g_Klebsiella*. Betaine, glutamic acid, N-stearoylsphinganine, PC(16:0/16:0), Pro-pro, 1-methyluric acid and Thr-Glu were negatively correlated with f_Tannerellaceae, f_Bacteroidaceae, *g_Parabacteroides* and *g_Bacteroides*. 13-Hydroxy-4z,7z,10z,14e,16z,19z-docosahexaenoic acid, prostaglandin a1 and stearaldehyde had obviously negative correlations with *g_Klebsiella*. 1,2-Dioleoyl-sn-glycero-3-phosphoethanolamine showed noteworthily negative correlations with o_Staphylococcales. These observations suggested that the alterations of NOP on differential metabolites were related to its regulations on gut microbiota, during exerting gastroprotective activity against AGML rats.

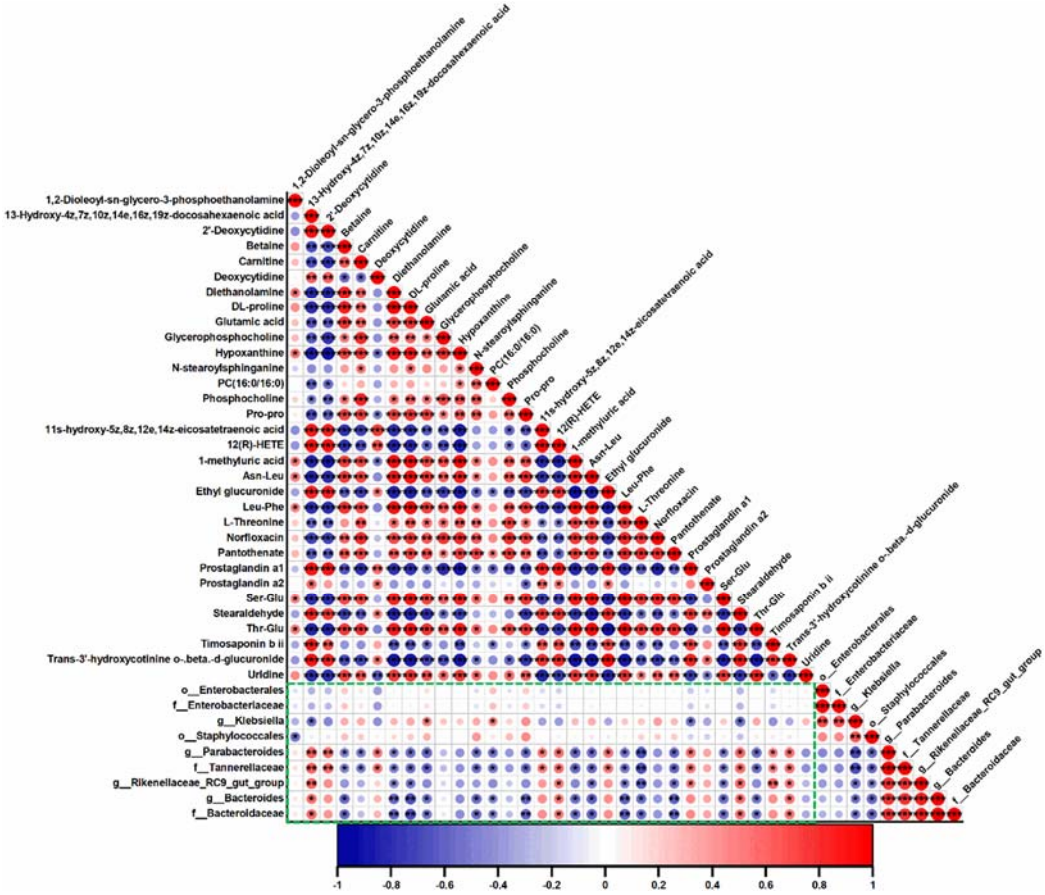

Fig. 9 Correlations between differential metabolites and gut microbiota of rats. $^{*}P < 0.05$, $^{**}P < 0.01$ and $^{***}P < 0.001$.

To the best of our knowledge, metabolites serve as key intermediaries in the health-promoting effects of most polysaccharides. The gastroprotective activities of several polysaccharides in rats or mice have been found to be closely related to their alterations on metabolites[11,13,16]. The relationships between biochemical indexes and differential metabolites affected by NOP are revealed in Fig. 10. Gastric lesion area ratio, TNF-α level, Il6 level, Ccl2 protein, Cxcl1 protein, Icam1 protein, Il6 protein, Jun protein and Lif protein were negatively correlated with diethanolamine and 1-methyluric acid, and were positively related to trans-3'-hydroxycotinine o-.beta.-d-glucuronide. 12(R)-HETE and ethyl glucuronide were positively correlated with gastric lesion area ratio, TNF-α level, Ccl2 protein, Cxcl1 protein, Icam1 protein, Il6 protein, Jun protein and Lif protein. 13-Hydroxy-4z,7z,10z,14e,16z,19z-docosahexaenoic acid and stearaldehyde showed positive correlations with gastric lesion area, Il6 level, Cxcl1 protein, Icam1 protein and Il6 protein.

Timosaponin b ii exhibited positive correlations with gastric lesion area ratio, Ccl2 protein, Cxcl1 protein, Icam1 protein and Il6 protein. 11s-Hydroxy-5z,8z,12e,14z-eicosatetraenoic acid displayed positive correlations with gastric lesion area ratio, TNF-α level, Il6 level, Icam1 protein and Il6 protein. 2'-Deoxycytidine revealed positive correlations with gastric lesion area ratio, Ccl2 protein and Cxcl1 protein. Prostaglandin a1 was positively correlated with gastric lesion area ratio, Cxcl1 protein and Il6 protein. Deoxycytidine was positively related to gastric lesion area ratio and TNF-α level. Hypoxanthine was negatively correlated with gastric lesion area ratio, TNF-α level, Ccl2 protein, Cxcl1 protein, Icam1 protein, Il6 protein, Jun protein and Lif protein. L-Threonine was negatively related to gastric lesion area ratio, TNF-α level, Il6 level, Ccl2 protein, Cxcl1 protein, Icam1 protein, Jun protein and Lif protein. DL-Proline showed negative correlations with gastric lesion area ratio, TNF-α level, Il6 level, Icam1 protein, Jun protein and Lif protein. Glutamic acid and Ser-Glu had negative correlations with gastric lesion area ratio, TNF-α level, Il6 level, Jun protein and Lif protein. Leu-Phe and Thr-Glu exhibited negative correlations with gastric lesion area ratio, TNF-α level, Il6 level, Jun protein and Lif protein. Betaine, Asn-Leu, pantothenate and uridine displayed negative correlations with gastric lesion area ratio, TNF-α level and Il6 level. Carnitine, Pro-pro and norfloxacin exerted negative correlations with gastric lesion area ratio and TNF-α level. N-stearoylsphinganine and phosphocholine revealed negative correlations with TNF-α level. These findings implied that the effects of NOP on biochemical indexes were related to its alterations on differential metabolites, during exhibiting gastroprotective activity against AGML rats.

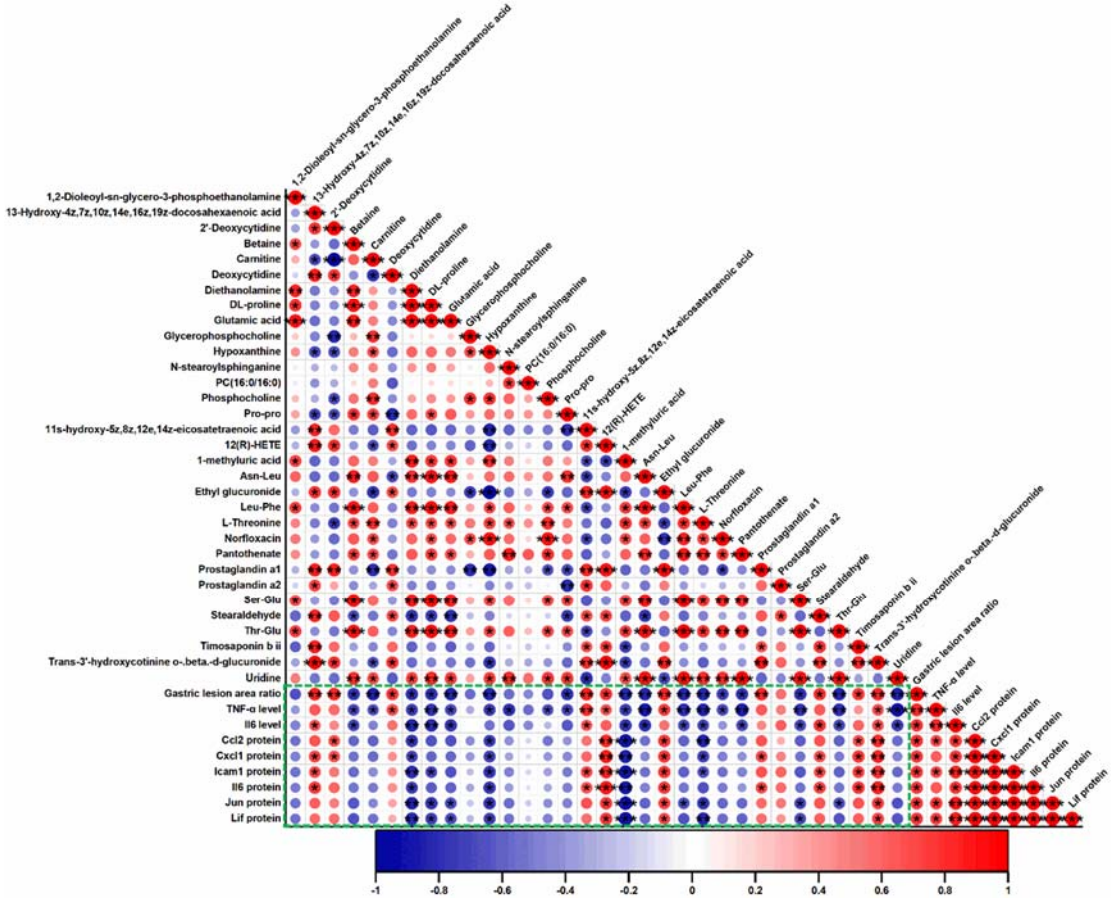

Fig. 10 Correlations between biochemical indexes and differential metabolites of rats. $^{*}P < 0.05$, $^{**}P < 0.01$ and $^{***}P < 0.001$.

3.8 Interactions between representative metabolites and inflammatory signaling pathways-related hub targets

Molecular docking was further performed to preliminarily explore whether NOP down-regulates inflammatory signaling pathways through the differential metabolites. In the Fig. 11, the bindings between six representative metabolites (diethanolamine, ethyl glucuronide, 12(R)-HETE, hypoxanthine, 1-methyluric acid and trans-3'-hydroxycotinine o-.beta.-d-glucuronide) and six inflammatory signaling pathways-related hub targets (Ccl2, Cxcl1, Icam1, Il6, Jun and Lif) are illustrated. In the Fig. 11(A), the molecular docking energies of the six metabolites and the six targets were -3.881~-2.796, -4.949~-4.483, -4.745~-3.670, -6.231~-4.101, -4.711~-5.118 and -6.828~-5.620 kcal/mol, successively. Binding energies less than -4.25 and -5.0 kcal/mol were considered as certain binding activity and good binding activity respectively[78]. The results indicated that ethyl glucuronide had certain binding activities with the six targets, and trans-3'-hydroxycotinine o-.beta.-d-glucuronide showed good binding activities with the six targets. However, diethanolamine had no certain binding activity with the six targets. Moreover, 12(R)-HETE had certain binding activities with Cxcl1, Icam1 and Jun, whilst it had no certain binding activity with Ccl2, Il6 and Lif. Hypoxanthine showed good binding activities with Il6 and Lif as well as certain binding activities with Ccl2 and Icam1, whereas it revealed no certain binding activity with Cxcl1 and Jun. 1-Methyluric acid exhibited good binding activities with Cxcl1, Icam1, Il6 and Jun, and certain binding activities with Ccl2 and Lif.

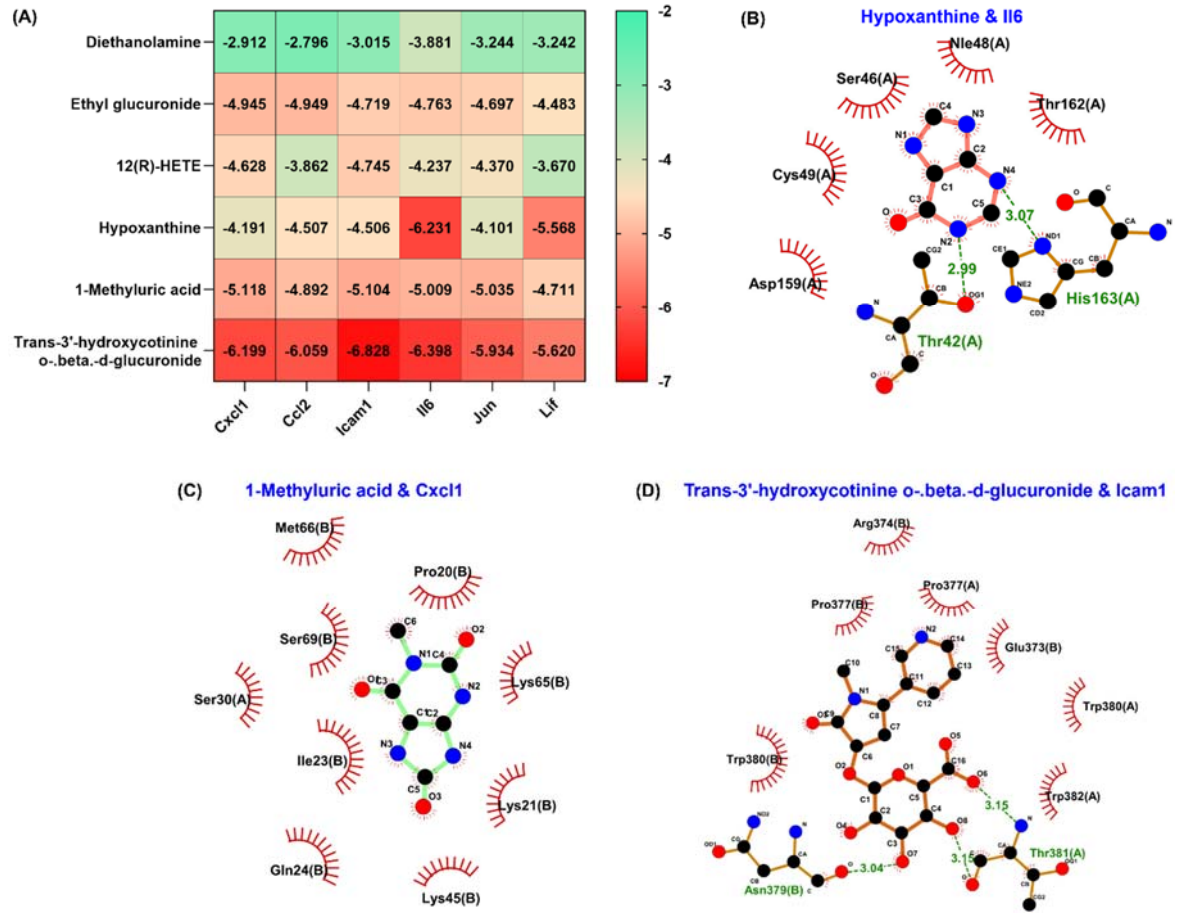

Fig. 11 Molecular docking results between representative metabolites and inflammatory signaling pathways-related hub targets. (A), heatmap of the molecular docking energy (kcal/mol); (B)~(D), 2D visualized interaction diagrams of hypoxanthine with Il6, 1-methyluric acid with Cxcl1, and trans-3'-hydroxycotinine o-.beta.-d-glucuronide with Icam1 obtained by molecular docking, successively.

Thereinto, the visualized interaction diagrams of hypoxanthine with Il6, 1-methyluric acid with Cxcl1, and trans-3'-hydroxycotinine o-.beta.-d-glucuronide with Icam1 are illustrated in Fig. 11(B)~Fig. 11(D). In the Fig. 11(B), hypoxanthine interacted with Il6 by hydrogen bonds to Thr42(A) and His163(A), and hydrophobic bonds to Asp159(A), Cys49(A), Ser46(A), Nle48(A) and Thr162(A). As shown in Fig. 11(C), 1-methyluric acid interacted with Cxcl1 through hydrophobic bonds to Ser30(A), Met66(B), Ser69(B), Ile23(B), Gln24(B), Pro20(B), Lys65(B), Lys21(B) and Lys45(B). In the Fig. 11(D), trans-3'-hydroxycotinine o-.beta.-d-glucuronide interacted with Icam1 via one hydrogen bond to Asn379(B) and two hydrogen bonds to Thr381(A), and hydrophobic bonds to Pro377(A), Trp380(A), Trp382(A), Glu373(B), Arg374(B), Pro377(B) and Trp380(B). These observations further indicated that the down-regulations of NOP on inflammatory signaling pathways might be realized through the differential metabolites, during exerting gastroprotective activity against AGML rats.

On the basis of above correlation analyses and molecular docking results, we could speculate: NOP might regulate gut microbiota (*g_Parabacteroides*, *g_Bacteroides*, *g_Klebsiella*, etc.) to produce metabolites (diethanolamine, hypoxanthine, 1-methyluric acid, etc.), then modulate inflammatory signaling pathways (TNF, IL-17, NF-κB and JAK-STAT signaling pathways) to exert anti-inflammatory (TNF-α and Il6 levels) effects, thereby alleviate AGML in rats. This speculation partly confirmed the reasonability of our aforementioned hypothesis in the Introduction section. In a previous study, mulberry fruit polysaccharides have been demonstrated to be digested by gastric and intestinal fluid[79]. A homogenous *Dendrobium huoshanense* polysaccharide (GXG) has been found to be degraded into a stable fragment (dGXG) in the stomach, where dGXG was propelled into the small intestine and absorbed into the systemic circulation[80]. Thus, the digestive behavior of NOP should be investigated to verify the proposed speculation in the future.

4. Conclusions

In the present study, a pectin NOP from Gannan navel orange (*Citrus sinensis* Osbeck cv. Newhall) peels was determined to consist of Results showed that NOP consisted of HG domain, RG-I domain and β-1,6-D-glucan structure. The side chains of RG-I domain were composed of →5)-α-L-Ara*f*-(1→, β-D-Gal*p*-(1→, →4)-β-D-Gal*p*-(1→ and →3,6)-β-D-Gal*p*-(1→ residues. This pectin was demonstrated to ameliorate gastric lesion, reduce inflammatory responses, down-regulate protein expressions of hub targets enriched in TNF, IL-17, NF-κB and JAK-STAT signaling pathways, alter metabolism of gastric tissues, and regulate gut microbiota in AGML rats. Moreover, significant correlations were observed among gut microbiota biomarkers, biochemical indexes and differential metabolites affected by NOP. Furthermore, some good binding activities were found between the representative metabolites and the inflammatory signaling pathways-related hub targets. This study supports the potential exploitation and utilization of NOP in preventing AGML, and lays a foundation for future investigation on gastroprotective mechanism of NOP. We proposed a speculation based on the findings: NOP might regulate gut microbiota to produce metabolites, in turn modulate inflammatory signaling pathways to exert anti-inflammatory effect, thereby alleviate AGML.

However, it has not been exactly validated, which is a shortcoming of this study. Our future work will focus on resolving this issue and exploring the behind mechanisms, along with understanding the digestive behavior of NOP.

Funding sources

This work was supported by the National Natural Science Foundation of China [32460589]; the Jiangxi Provincial Natural Science Foundation [20252BAC240617 & 20202BABL216081 & 20232BAB215062]; the University-Level Scientific Research Projects of Gannan Medical University [QD201913, QD202013, QD202128, TD202313 & TD202313-1]; the Jiangxi Provincial Fuzhou Project under Open Competition Mechanism [2023JDB024]; and the Open Project of Key Laboratory of Prevention and Treatment of Cardiovascular and Cerebrovascular Diseases, Ministry of Education (XN201932).

Acknowledgments

The authors greatly appreciated the technical services of Applied Protein Technology Co., Ltd. (Shanghai, China) in detections and data analyses of RNA-seq, gut microbiota and untargeted metabolomics.

Declaration of competing interest

The authors declared that they have no conflict of interest.

References

[1] World Health Organization, Global status report on alcohol and health 2018, World Health Organization. (2019).

[2] J.E. Yoo, D.W. Shin, K. Kim, et al., Association of the frequency and quantity of alcohol consumption with gastrointestinal cancer, JAMA Netw. Open. 4(8) (2021) e2120382. https://doi.org/10.1001/jamanetworkopen.2021.20382.

[3] A.M. Vilcu, L. Sabatte, T. Blanchon, et al., Association between acute gastroenteritis and continuous use of proton pump inhibitors during winter periods of highest circulation of enteric viruses, JAMA Netw. Open. 2(11) (2019) e1916205. https://doi.org/10.1001/jamanetworkopen.2019.16205.

[4] X.Y. Wang, J.Y. Yin, J.L. Hu, et al., Gastroprotective polysaccharide from natural sources: Review on structure, mechanism, and structure-activity relationship, Food Frontiers. 3(4) (2022) 560-591. https://doi.org/10.1002/fft2.172.

[5] M.Z. Guo, H.F. Yu, M. Meng, et al., Research on the structural characteristics of a novel *Chinese Iron Yam* polysaccharide and its gastroprotection mechanism against ethanol-induced gastric mucosal lesion in a BALB/c mouse model, Food Funct. 11(7) (2020) 6054-6065. https://doi.org/10.1039/c9fo02642h.

[6] Y.Z. Liu, D.Y. Sui, W.W. Fu, et al., Protective effects of polysaccharides from *Panax ginseng* on acute gastric ulcers induced by ethanol in rats, Food Funct. 12(6) (2021) 2741-2749. https://doi.org/10.1039/d0fo02947e.

[7] H.Y. Ye, Z.Z. Shang, Z.Q. Zhang, et al., *Dendrobium huoshanense* stem polysaccharide ameliorates alcohol-induced gastric ulcer in rats through Nrf2-mediated strengthening of gastric mucosal barrier, Int. J. Biol. Macromol. 236 (2023) 124001. https://doi.org/10.1016/j.ijbiomac.2023.124001.

[8] X.M. Zhang, D. Liu, Z.Y. Ye, et al., Gastroprotective effect of the *Lachnum* polysaccharide and polysaccharide-dipeptide conjugates against gastric ulcer, Food Chem. Toxicol. 174 (2023) 113661. https://doi.org/10.1016/j.fct.2023.113661.

[9] H. Zhu, L. Xu, P. Chen, et al., Structure characteristics, protective effect and mechanisms of ethanol-fractional polysaccharides from *Dendrobium officinale* on acute ethanol-induced gastritis, Food Funct. 15(8) (2024) 4079-4094. https://doi.org/10.1039/D3FO05540J.

[10] J.F. Wardman, R.K. Bains, P. Rahfeld, et al., Carbohydrate-active enzymes (CAZymes) in the gut microbiome, Nat. Rev. Microbiol. 20(9) (2022) 542-556. https://doi.org/10.1038/s41579-022-00712-1.

[11] Z.Y. Huang, M.W. Hu, X.Y. Peng, et al., The protective effect of small black soybean (*Vigna mungo* L.) polysaccharide on acetic acid-induced gastric ulcer in SD rats and its impact on gut microbiota and metabolites, Food Biosci. 56 (2023) 103187. https://doi.org/10.1016/j.fbio.2023.103187.

[12] D.J. Zhang, M. Xiang, Y. Jiang, et al., The protective effect of polysaccharide SAFP from *Sarcodon aspratus* on water immersion and restraint stress-induced gastric ulcer and modulatory effects on gut microbiota dysbiosis, Foods. 11(11) (2022) 1567. https://doi.org/10.3390/foods11111567.

[13] J.H. Luo, W.S. Zou, J. Li, et al., Untargeted serum and liver metabolomics analyses reveal the gastroprotective effect of polysaccharide from *Evodiae fructus* on ethanol-induced gastric ulcer in mice, Int. J. Biol. Macromol. 232 (2023) 123481. https://doi.org/10.1016/j.ijbiomac.2023.123481.

[14] B. Luo, M.G. Cai, H.Y. Huang, et al., A pectic polysaccharide from wax gourd peel improves ethanol-induced gastric ulcer injury in mice via the PI3K/AKT signaling pathway, Int. J. Biol. Macromol. 316(Pt 2) (2025) 144755. https://doi.org/10.1016/j.ijbiomac.2025.144755.

[15] P. Liu, Z. Zhang, M.J. Du, et al., Restoring mitochondrial function and remodeling gut microbiota by low-molecular-weight β-glucan of *Hericium erinaceus* in alcohol-induced gastrointestinal injury, J. Agr. Food Chem. 73(45) (2025) 28864-28882.

[16] X.Y. Wang, M. Hao, Y.P. Li, et al., Structural characteristics of a purified *Evodiae fructus* polysaccharide and its gastroprotection and relevant mechanism against alcohol-induced gastric lesions in rats, Int. J. Biol. Macromol. 281(Pt3) (2024) 136410. https://doi.org/10.1016/j.ijbiomac.2024.136410.

[17] S.G. Li, A.R. Tan, Y.X. Li, et al., Polysaccharides from *Hippophae rhamnoides* L. protected against ethanol-induced gastric ulcer in mice and its impact on metabolites and gut microbiota, Int. J. Biol. Macromol. 221(Pt2) (2025) 117336. https://doi.org/10.1016/j.foodres.2025.117336.

[18] Y. Yuan, Y.Y. Duan, Y.Q. Zhang, et al., Untargeted metabolomics analysis of Gannan navel orange at different storage periods under room temperature using HS-SPME-GC-MS and UPLC-Q-TOF/MS, Food Chem. 440 (2024) 138186. https://doi.org/10.1016/j.foodchem.2023.138186.

[19] J.Q. Sang, L. Li, J. Wen, et al., Evaluation of the structural, physicochemical and functional properties of dietary fiber extracted from newhall navel orange by-products, Foods. 10(11) (2021) 2772. https://doi.org/10.3390/foods10112772.

[20] N.A. Patience, D. Schieppati, D.C. Boffito, Continuous and pulsed ultrasound pectin extraction from navel orange peels, Ultrason. Sonochem. 73 (2021) 105480. https://doi.org/10.1016/j.ultsonch.2021.105480.

[21] H.L. Dong, T.T. Dai, L. Liang, et al., Physicochemical properties of pectin extracted from navel orange peel dried by vacuum microwave, LWT-Food Sci. Technol. 151 (2021) 112100. https://doi.org/10.1016/j.lwt.2021.112100.

[22] X.F. Guo, D.M. Han, H.P. Xi, et al., Extraction of pectin from navel orange peel assisted by ultra-high pressure, microwave or traditional heating: A comparison, Carbohyd. Polym. 88(2) (2012) 441-448. https://doi.org/10.1016/j.carbpol.2011.12.026.

[23] T.M. Cantu-Jungles, D. Maria-Ferreira, L.M. da Silva, et al., Polysaccharides from prunes: gastroprotective activity and structural elucidation of bioactive pectins, Food Chem. 146 (2014) 492-499. https://doi.org/10.1016/j.foodchem.2013.09.093.

[24] M.L. Corrêa-Ferreira, D.M. Ferreira, J.L. Dallazen, et al., Gastroprotective effects and structural characterization of a pectic fraction isolated from *Artemisia campestris subsp maritima*, Int. J. Biol. Macromol. 107(PtB) (2018) 2395-2403. https://doi.org/10.1016/j.ijbiomac.2017.10.127.

[25] A.F. de Oliveira, B.B. da Luz, M.F.P. Werner, et al., Gastroprotective activity of a pectic polysaccharide fraction obtained from infusion of *Sedum dendroideum* leaves, Phytomedicine. 41 (2018) 7-12. https://doi.org/10.1016/j.phymed.2018.01.015.

[26] A.M. Nascimento, D. Maria-Ferreira, E.F. de Souza, et al., Gastroprotective effect and chemical characterization of a polysaccharide fraction from leaves of *Croton cajucara*, Int. J. Biol. Macromol. 95 (2017) 153-159. https://doi.org/10.1016/j.ijbiomac.2016.11.044.

[27] T. Liang, J.W. Hu, H. Song, et al., Comparative study on physicochemical characteristics, α-glucosidase inhibitory effect, and hypoglycemic activity of pectins from normal and Huanglongbing-infected navel orange peels, J. Food Biochem. 46(10) (2022) e14280. https://doi.org/10.1111/jfbc.14280.

[28] Q.B. Guo, J.H. Du, Y. Jiang, et al., Pectic polysaccharides from hawthorn: Physicochemical and partial structural characterization, Food Hydrocolloid. 90 (2019) 146-153. https://doi.org/10.1016/j.foodhyd.2018.10.011.

[29] X.Y. Wang, R. Xu, J.Y. Yin, et al., Physicochemical, structural and rheological properties of alkali-extracted polysaccharide from fruiting body of *Hericium erinaceus*, LWT-Food Sci. Technol. 115 (2019) 108330. https://doi.org/10.1016/j.lwt.2019.108330.

[30] Q.Y. Chen, Y. Wang, N. Yin, et al., Polysaccharides from fermented wheat bran enhanced the growth performance of zebrafish (*Danio rerio*) through improving gut microflora and antioxidant status, Aquacult. Rep. 25 (2022) 101188. https://doi.org/10.1016/j.aqrep.2022.101188.

[31] J.Y. Huang, Q. Zou, M. Hao, et al., Exploring the potential mechanisms of polysaccharides against gastric ulcer: Network pharmacology analysis and molecular docking validation, Food Safe. Health. 3(2) (2025) 232-249. https://doi.org/10.1002/fsh3.12079.

[32] J. Eberhardt, D. Santos-Martins, A.F. Tillack, et al., AutoDock Vina 1.2.0: New docking methods, expanded force field, and python bindings, J. Chem. Inf. Model. 61(8) (2021) 3891-3898. https://doi.org/10.1021/acs.jcim.1c00203.

[33] O. Trott, A.J. Olson, AutoDock Vina: improving the speed and accuracy of docking with a new scoring function, efficient optimization, and multithreading, J. Comput. Chem. 31(2) (2010) 455-461. https://doi.org/10.1002/jcc.21334.

[34] R.Z. Chen, S.J. Luo, C.X. Wang, et al., Effects of ultra-high pressure enzyme extraction on characteristics and functional properties of red pitaya (*Hylocereus polyrhizus*) peel pectic polysaccharides, Food Hydrocolloid. 121 (2021) 107016. https://doi.org/10.1016/j.foodhyd.2021.107016.

[35] Y.S. Cui, Y.X. Li, S.L. Jiang, et al., Isolation, purification, and structural characterization of polysaccharides from *Atractylodis Macrocephalae Rhizoma* and their immunostimulatory activity in RAW264.7 cells, Int. J. Biol. Macromol. 163 (2020) 270-278. https://doi.org/10.1016/j.ijbiomac.2020.06.269.

[36] W.B. Chen, X.L. Zhu, J.J. Ma, et al., Structural elucidation of a novel pectin-polysaccharide from the petal of *Saussurea laniceps* and the mechanism of its anti-HBV activity, Carbohyd. Polym. 223 (2019) 115077. https://doi.org/10.1016/j.carbpol.2019.115077.

[37] L.L. Huang, J. Zhao, Y.L. Wei, et al., Structural characterization and mechanisms of macrophage immunomodulatory activity of a pectic polysaccharide from *Cucurbita moschata* Duch, Carbohyd. Polym. 269 (2021) 118288. https://doi.org/10.1016/j.carbpol.2021.118288.

[38] H.N. Su, L.L. He, X.N. Yu, et al., Structural characterization and mechanisms of macrophage immunomodulatory activity of a novel polysaccharide with a galactose backbone from the processed *Polygonati Rhizoma*, J. Pharm. Anal. 14(7) (2024) 100974. https://doi.org/10.1016/j.jpha.2024.100974.

[39] R. Guo, J.A. Zhang, X. Liu, et al., Pectic polysaccharides from Biluochun Tea: A comparative study in macromolecular characteristics, fine structures and radical scavenging activities in vitro, Int. J. Biol. Macromol. 195 (2022) 598-608. https://doi.org/10.1016/j.ijbiomac.2021.12.004.

[40] S.H. Deng, T.F. Zhang, S.H. Fan, et al., Polysaccharide conjugates' contribution to mellow and thick taste of Pu-erh ripe tea, besides Theabrownin, Food Chem. X. 23 (2024) 101726. https://doi.org/10.1016/j.fochx.2024.101726.

[41] Z.Y. Zhu, X.Y. Song, Y.Z. Jiang, et al., Chemical structure and antioxidant activity of a neutral polysaccharide from *Asteris Radix et Rhizoma*, Carbohyd. Polym. 286 (2022) 119309. https://doi.org/10.1016/j.carbpol.2022.119309.

[42] Z.H. Bi, Y. Zhao, J.H. Hu, et al., A novel polysaccharide from *Lonicerae Japonicae Caulis*: Characterization and effects on the function of fibroblast-like synoviocytes, Carbohyd. Polym. 292 (2022) 119674. https://doi.org/10.1016/j.carbpol.2022.119674.

[43] X. Zhang, S. Liu, F.G Kong, et al., Acidic polysaccharide from *Ganoderma tsugae*: Structural characterization and antiatherosclerotic related to macrophage polarization, Food Res. Int. 203 (2025) 115913. https://doi.org/10.1016/j.foodres.2025.115913.

[44] J.H. Sun, T.T. Yan, Y.Y. Zhang, et al., Gastroprotective effect of fucoidan from *Sargassum siliquastrum* against ethanol-induced gastric mucosal injury, Food Res. Int. 201 (2025) 115566. https://doi.org/10.1016/j.foodres.2024.115566.

[45] Z.Y. Zhang, H.L. Xie, M.A. Farag, et al., *Dendrobium officinale* flowers flavonoids enriched extract protects against acute ethanol-induced gastric ulcers via AMPK/PI3K signaling pathways, Food Sci. Hum. Well. 13(6) (2024) 3661-3679. https://doi.org/10.26599/FSHW.2023.9250048.

[46] H.Q. Sun, Y.Y. Zhang, J.H. Zhang, et al., Gastroprotective effects of polysaccharides from purple sweet potato (*Ipomoea batatas* (L.) Lam) on an ethanol-induced gastric ulcer via regulating immunity and activating the PI3K/Akt/Rheb/mTOR pathway, Food Funct. 15(12) (2024) 6408-6423. https://doi.org/10.1039/D4FO01071J.

[47] R.R. Yang, J.J. Li, C.M. Jiang, et al., Preventive and therapeutic effects of an exopolysaccharide produced by *Lacticaseibacillus rhamnosus* on alcoholic gastric ulcers, Int. J. Biol. Macromol. 235 (2023) 123845. https://doi.org/10.1016/j.ijbiomac.2023.123845.

[48] Y.L. Zhang, Y. Li, F.X. An, et al., *Peucedanum praeruptorum* Dunn leaf aqueous extract protects against alcoholic gastric injury by inhibiting inflammation and oxidative stress in mice, J. Ethnopharmacol. 335 (2024) 118628. https://doi.org/10.1016/j.jep.2024.118628.

[49] T.A. Sebrell, M. Hashimi, B. Sidar, et al., A novel gastric spheroid co-culture model reveals chemokine-dependent recruitment of human dendritic cells to the gastric epithelium, Cell. Mol. Gastroenter. 8(1) (2019) 157-171.e3. https://doi.org/10.1016/j.jcmgh.2019.02.010.

[50] R.H. Ni, Y. Luo, L.J. Jiang, et al., Repairing gastric ulcer with hyaluronic acid/extracellular matrix composite through promoting M2-type polarization of macrophages, Int. J. Biol. Macromol. 245 (2023) 125556. https://doi.org/10.1016/j.ijbiomac.2023.125556.

[51] M.D. Giraldez, D. Carneros, C. Garbers, et al., New insights into IL-6 family cytokines in metabolism, hepatology and gastroenterology, Nat. Rev. Gastro. Hepat. 18(11) (2021) 787-803. https://doi.org/10.1038/s41575-021-00473-x.

[52] P. Huang, W.H. Tang, R. Shen, et al., Analysis of candidate biomarkers and related transcription factors involved in the development and restoration of stress-induced gastric ulcer by transcriptomics, Cell Stress Chaperon. 25(2) (2020) 265-275. https://doi.org/10.1007/s12192-020-01070-8.

[53] G.F. Asaad, R.E. Mostafa, Lactoferrin mitigates ethanol-induced gastric ulcer via modulation of ROS/ICAM-1/Nrf2 signaling pathway in Wistar rats, Iran. J. Basic. Med. Sci. 25(12) (2022) 1522-1527. https://doi.org/10.22038/IJBMS.2022.66823.14656.

[54] Y.Z. Lian, I.H. Lin, Y.C. Yang, et al., Gastroprotective effect of *Lycium barbarum* polysaccharides and C-phycocyanin in rats with ethanol-induced gastric ulcer, Int. J. Biol. Macromol. 165(PtA) (2020) 1519-1528. https://doi.org/10.1016/j.ijbiomac.2020.10.037.

[55] K. Tanaka, Y. Tanaka, T. Suzuki, et al., Protective effect of β-(1,3 →1,6)-D-glucan against irritant-induced gastric lesions, Brit. J. Nutr. 106(4) (2011) 475-485. https://doi.org/10.1017/S0007114511000365.

[56] S.B. Ma, Q. Wu, Z.L. Zhao, et al., Mechanisms of *Dendrobium officinale* polysaccharides in repairing gastric mucosal injuries based on mitogen-activated protein kinases (MAPK) signaling pathway, Bioengineered. 13(1) (2022) 71-82. https://doi.org/10.1080/21655979.2021.2006951.

[57] F. Wang, C. Yuan, R. Deng, et al., Multi-omics analysis reveals the pre-protective mechanism of *Dendrobium flexicaule* polysaccharide against alcohol-induced gastric mucosal injury, Int. J. Biol. Macromol. 291 (2025) 139191. https://doi.org/10.1016/j.ijbiomac.2024.139191.

[58] D. Dokmeci, M. Akpolat, N. Aydogdu, et al., L-carnitine inhibits ethanol-induced gastric mucosal injury in rats, Pharmacol. Rep. 57(4) (2005) 481-488.

[59] B.S. Dunjic, J. Axelson, A. Ar'Rajab, et al., Gastroprotective capability of exogenous phosphatidylcholine in experimentally induced chronic gastric ulcers in rats, Scand. J. Gastroentero. 28(1) (1993) 89-94. https://doi.org/10.3109/00365529309096051.

[60] B. Ganesan, R. Yathavamoorthi, K.S.H. Farvin, et al., Supplementation of betaine attenuates HCl-ethanol induced gastric ulcer in rats, Int. J. Biol. Chem. 4(2) (2010) 79-89. https://doi.org/10.3923/ijbc.2010.79.89.

[61] J.X. Wen, Y.L. Tong, X. Ma, et al., Therapeutic effects and potential mechanism of dehydroevodiamine on N-methyl-N'-nitro-N-nitrosoguanidine-induced chronic atrophic gastritis, Phytomedicine. 91 (2021) 153619. https://doi.org/10.1016/j.phymed.2021.153619.

[62] Z.X. Xu, H.M. Zhang, Y.Z. Yang, et al., Camellia oil (*Camellia oleifera* Abel.) alleviates gastric injury induced by ethanol associated with modulation of gut microbiota in mice, Oil. Crop. Sci. 8(1) (2023) 61-71. https://doi.org/10.1016/j.ocsci.2023.02.006.

[63] S.H. Wu, X. Chen, H.H. Liu, et al., Study of Zuojin Pill in treating chronic atrophic gastritis by UPLC-Q-TOF/MS based on serum and urine metabolomics combined with network pharmacology, Int. J. Anal. Chem. 2021(1) (2021) 6649600. https://doi.org/10.1155/2021/6649600.

[64] Y. Gao, Inflammation and gut microbiota in the alcoholic liver disease, Food Med. Homol. 1(2) (2024) 9420020. https://doi.org/10.26599/FMH.2024.9420020.

[65] L Guo, Q.Y. Ding, W.H. Duan, et al., Goji-derived exosomes-like nanoparticles ameliorate alcohol-induced acute liver injury by modulating gut microbiota and metabolites, Food Med. Homol. 3(1) (2026) 9420081. https://doi.org/10.26599/FMH.2026.9420081.

[66] A.P. Oliveira, L.K.M. Souza, T.S.L. Araújo, et al., *Lactobacillus reuteri* DSM 17938 protects against gastric damage induced by ethanol administration in mice: Role of TRPV1/substance P axis, Nutrients. 11(1) (2019) 208. https://doi.org/10.3390/nu11010208.

[67] C.C. Yang, Y. Du, D.Y. Ren, et al., Gut microbiota-dependent catabolites of tryptophan play a predominant role in the protective effects of turmeric polysaccharides against DSS-induced ulcerative colitis, Food Funct. 12(20) (2021) 9793-9807. https://doi.org/10.1039/d1fo01468d.

[68] P. Dharmani, C. De Simone, K. Chadee, The probiotic mixture VSL#3 accelerates gastric ulcer healing by stimulating vascular endothelial growth factor, PLoS. One. 8(3) (2013) e58671. https://doi.org/10.1371/journal.pone.0058671.

[69] J. Zhang, Y.Q. Hu, L.D. Wu, et al., Causal effect of gut microbiota on gastroduodenal ulcer: a two-sample Mendelian randomization study, Front. Cell. Infect. Microbiol. 13 (2023) 1322537. https://doi.org/10.3389/fcimb.2023.1322537.

[70] C. Wang, X. Yu, H.Q. Lin, et al., Integrating microbiome and metabolome revealed microbe-metabolism interactions in the stomach of patients with different severity of peptic ulcer disease, Front. Immunol. 14 (2023) 1134369. https://doi.org/10.3389/fimmu.2023.1134369.

[71] X.D. Li, Y.X. Fei, X.M. Luo, et al., Mechanism of *Phyllanthus emblica* polyphenols in alleviating DSS-induced ulcerative colitis: Insights from transcriptomics and microbiome analysis, Food Biosci. 61 (2024) 104886. https://doi.org/10.1016/j.fbio.2024.104886.

[72] F. Peng, Z.Q. Yu, B. Du, et al., Non-starch polysaccharides from *Castanea mollissima Bl.* ameliorate metabolic syndrome by remodeling barrier function, microbial community, and metabolites in high-fat-diet/streptozotocin-induced diabetic mice, Food Res. Int. 202 (2025) 115638. https://doi.org/10.1016/j.foodres.2024.115638.

[73] L. Wang, Z.H. Zhang, Z.K. Zeng, et al., Structural characterization of polysaccharide from an edible fungus *Dictyophora indusiata* and the remodel function of gut microbiota in inflammatory mice, Carbohyd. Polym. 351 (2025) 123141. https://doi.org/10.1016/j.carbpol.2024.123141.

[74] W.Y Fan, X.X Fan, Y.J Xie, et al., Research progress on the anti-aging effects and mechanisms of polysaccharides from Chinese herbal medicine, Food Med. Homol. 3(1) (2026) 9420108. https://doi.org/10.26599/FMH.2026.9420108.

[75] E.J. Ning, C.W. Sun, X.F. Wang, et al., *Artemisia argyi* polysaccharide alleviates intestinal inflammation and intestinal flora dysbiosis in lipopolysaccharide-treated mice, Food Med. Homol. 1(1) (2024) 9420008. https://doi.org/10.26599/FMH.2024.9420008.

[76] D.D. Zhang, J. Liu, H. Cheng, et al., Interactions between polysaccharides and gut microbiota: A metabolomic and microbial review, Food Res. Int. 160 (2022) 111653. https://doi.org/10.1016/j.foodres.2022.111653.

[77] A.U. Hasan, A. Rahman, H. Kobori, Interactions between host PPARs and gut microbiota in health and disease, Int. J. Mol. Sci. 20(2) (2019) 387. https://doi.org/10.3390/ijms20020387.

[78] C. Li, R. Wen, D.W. Liu, et al., Assessment of the potential of *Sarcandra glabra (Thunb.)* Nakai. in treating ethanol-induced gastric ulcer in rats based on metabolomics and network analysis, Front. Pharmacol. 13 (2022) 810344. https://doi.org/10.3389/fphar.2022.810344.

[79] C. Chen, B. Zhang, X. Fu, et al., The digestibility of mulberry fruit polysaccharides and its impact on lipolysis under simulated saliva, gastric and intestinal conditions, Food Hydrocolloid. 58 (2016) 171-178. https://doi.org/10.1016/j.foodhyd.2016.02.033.

[80] S.Z. Xie, J.C. Ge, F. Li, et al., Digestive behavior of *Dendrobium huoshanense* polysaccharides in the gastrointestinal tracts of mice, Int. J. Biol. Macromol. 107(Part A) (2018) 825-832. https://doi.org/10.1016/j.ijbiomac.2017.09.047.